

Contents lists available at ScienceDirect

Energy

journal homepage: www.elsevier.com/locate/energy



Maximum thermal efficiencies of supercritical CO_2 power cycle at various power capacities



Tianze Wang^a, Jinliang Xu^{a,b,*}, Guanglin Liu^{a,b}

- a Beijing Key Laboratory of Multiphase Flow and Heat Transfer for Low Grade Energy Utilization, North China Electric Power University, Beijing, 100026, China
- b Key Laboratory of Power Station Energy Transfer Conversion and System (North China Electric Power University), Ministry of Education, Beijing, 102206, China

ARTICLE INFO

Handling editor: Ruzhu Wang

Keywords: sCO₂ cycle Thermal efficiency Power capacity Optimal parameters

ABSTRACT

Herein, we investigate the relationships between efficiencies $\eta_{\rm th}$, main vapor parameters (P_5 and T_5) and power capacities ($W_{\rm net}$) on coal-fired supercritical carbon dioxide cycle (sCO₂). We developed a model to couple the cycle and the components. The overlap energy strategy and boiler module design reduce the efficiency penalty. The multi-stages axial turbines and compressors were modeled to explore their performance as $W_{\rm net}$ changes. For given $W_{\rm net}$, $\eta_{\rm th}$ increases as T_5 increases. However, $\eta_{\rm th}$ displays parabolic distribution versus P_5 , due to the tradeoff between the decreased pressure drop of sCO₂ boilers and the increased compression power, as P_5 raises. Then, for fixed T_5 given by the tolerance limit of materials, the monotonous increase of the optimal P_5 with increase of $W_{\rm net}$ is found, due to the decreased pressure drops of sCO₂ boiler as positive effect suppressing the increased compression power as negative effect. Finally, with $W_{\rm net}$ in the range of (100–1000) MWe, the system efficiency is found to increase as $W_{\rm net}$ increases, matching the scale law regarding efficiencies with respect to system sizes. Our work concludes important roles of boiler pressure drops and compression work on system, providing the guidance to select the "optimal" power capacity that has the "best" system performance.

1. Introduction

The supercritical carbon dioxide (sCO₂) cycle is attractive for green energy utilization. Electric supply demands a reduction in the consumption of fossil fuels and increased utilization of renewable energy [1]. The electric grid operates in a mixed mode, including fossil fuel, renewable, and nuclear energy. Classically, the water-steam Rankine cycle has been widely used for thermal power conversion. These Rankine cycle power plants respond slowly to load variations, which is not beneficial for the adoption of unstable renewable energies [2]. Compared with the water-steam Rankine cycle power plants, the sCO₂ cycle has received great attention because it not only has higher efficiencies but also quickly responds to load variations [3].

Several studies have been conducted on the sCO_2 cycle, including cycle analyses and component development [4–7]. Engineers would like to know whether there is an optimal power capacity (W_{net}) at which the thermal efficiency reaches a maximum or how the thermal efficiencies are influenced by the W_{net} . To address this issue, let us first review the conclusions drawn from the water-steam Rankine cycle. Bejian et al. [8] used thermodynamics to demonstrate why larger flow systems were

more efficient than smaller ones. This is because larger systems have larger flow passages and heat transfer surfaces and do not strangle the currents that must flow. Constructal-design features form the basis for scaling up and scaling down the configurations of flow systems.

China has made significant efforts to increase the efficiency of thermal power plants since the 1950s [9]. For coal-fired power plants, the $W_{\rm net}$ has four levels: 100, 300, 600, and 1000 MWe [10,11]. Fig. 4 in ref. [12] shows that the net thermal efficiency increases linearly with an increase in the $W_{\rm net}$ factor for both China and the United States. Meanwhile, the main vapor state changes from subcritical to supercritical pressure [13].

The main vapor parameters are key to influencing the thermal efficiency of the system. An increase in the main vapor temperature, utilization of reheating, and reheating temperature can increase thermal efficiencies [14]. For ultra-supercritical steam power generation, the following conclusions were drawn: (1) The thermal efficiency increases as the main vapor temperature increases. For example, thermal efficiency can increase by 0.25 %–0.30 % as the main vapor temperature increases by 10 $^{\circ}$ C [15]. (2) The main vapor pressures have a complicated effect on thermal efficiencies. The thermal efficiencies simultaneously increased with an increase in the main vapor temperature and

E-mail address: xjl@ncepu.edu.cn (J. Xu).

^{*} Corresponding author. Beijing Key Laboratory of Multiphase Flow and Heat Transfer for Low Grade Energy Utilization, North China Electric Power University, Beijing, 100026, China.

Nomenclature		Δ	roughness (mm)
	. 2.	σ	solidity
A	area (m²)	γ	stagger angle (°)
b	Blade height (m)	η_{C} , η_{T}	turbomachinery efficiency
c	chord length (m)	$\eta_{ m th}$	thermal efficiency
$d_{ m i}$	internal diameter of pipe (mm)	arepsilon	pressure ratio, relative error
$d_{ m m}$	mean radius (mm)	α	absolute flow angle (°)
e	exergy per unit mass (kJ/kg)	eta	relative flow angle (°)
f	friction coefficient	λ	ratio of hub radius to tip radius
g	gravitational acceleration	ρ	density (kg/m³)
G	mass velocity (kg/m ² s)	μ	viscosity (Pa·s)
h	enthalpy (J/kg)	C-1	4-
I	exergy loss (MW)	Subscrip	
L	lenght (m)	1,2,3	state point
m	mass flow rate (kg/s)	a	acceleration pressure drop
n	speed (r/min)	C	compressor
N	number of stages	cl	clearance loss
$N_{ m S}$	specific speed	f	friction
P	pressure (MPa)	g	gravity pressure drop
$Q_{ m total}$	heat	i	inlet
Q	volume flow rate (m ³ /s)	max	maximum
R	degree of reaction	net	unit capacity
Re	Reynolds number	0	outlet
s	entropy (kJ/kg)	op	optimal
t	trailing edge (m)	p	profile loss
T	temperature (°C)	part	part of heater
t _{max}	maximum trailing edge (m)	R	rotor
U	peripheral speed (m/s)	S	stator
V	flow velocity (m/s)	S	secondary loss
W	power capacity (MW)	SS	ideal value
$W_{\rm max}$	maximum flow velocity (m/s)	T	turbine
$W_{ m RE}$	equivalent speed ratios	te	trailing edge loss
$W_{ m RE}^{ m min}$	stall speed ratios		
Y RE	irreversible loss	Abbrevio	
Y	irreversible loss	EAP	external air preheater
Greek symbols		HTR	high temperature heat exchanger
ΔP	pressure drop (MPa)	LTR	low temperature heat exchanger
θ	camber angle (°)	PCHE	printed circuit heat exchanger
φ	flow coefficient	PFM	partial flow mode
Ψ	loading coefficient	SH	superheater

pressure. However, by fixing the main vapor temperature, an increase in the main vapor pressure alone deteriorates system performance [16].

It is doubtful that the above conclusions, drawn from the water-steam Rankine cycle, are correct for the sCO₂ power cycle for the following reasons: (1) The sCO₂ cycle is completely different from the water-steam Rankine cycle. The former uses a compressor to supply the pressure head and overcome the pressure drop across the entire system. A larger amount of compression work is required than the pumping power for the Rankine cycle [17]. (2) The boiler drove the system to generate power. Owing to the ultra-large circulating flow rates, the sCO₂ boiler should be decoupled into a set of modules operating in the partial flow mode to decrease pressure drops [18]. (3) A large heat recovery is necessary for the sCO₂ cycle. Usually, the thermal load during the internal heat recovery process is approximately three to four times the net power generated by the system [19]. (4) The sCO₂ turbine had a different configuration than the water-steam turbine. These two types of machines exhibit different responses with respect to their main vapor parameters [20].

For the sCO₂ cycle, the relationship between the thermal efficiencies, main vapor parameters, and power capacities has not been previously reported. Available studies have focused on the dependence of thermal efficiencies on the main vapor parameters at fixed power capacities,

mass flow rates [21-23] and their thermal efficiencies depend on the power capacities with identical main vapor parameters [24,25]. The objective of this study is to fill this gap. Liu et al. [24] highlighted the penalty effect of an ultra-large pressure drop on the system performance with power capacities in the range of (50-1000) MWe. To eliminate this penalty effect, a partial flow mode (PFM) is proposed instead of a total flow mode (TFM). For the PFM applications, the CO2 stream was segmented into two parallel lines, each with half the flow rate and half the length. They concluded that with an increase in W_{net} , the TFM significantly elevates pressure drops, not only increasing energy loads, but also increasing exergy destruction for all components, deteriorating the first and second law efficiencies of the system. Compared with the TFM, the PFM reduces pressure drops. Cycles using the PFM had much higher efficiencies than those using the TFM. At a smaller W_{net} such as 100 MWe, sCO₂ boiler has larger surface-to-volume ratio, and the flow passages of CO₂ were sufficient to maintain an acceptable pressure drop. Hence, the system performance was similar for both TFM and PFM. It has been shown that the flow splitting strategy is necessary for W_{net} > 100 MWe and is not recommended only at very small power capacities, such as W_{net}< 100 MWe. The effect of the power capacity, W_{net}, on the performance of sCO2 coal-fired power plants was investigated by Wang et al. [25], with W_{net} in the range of (100-1000) MWe. The thermal

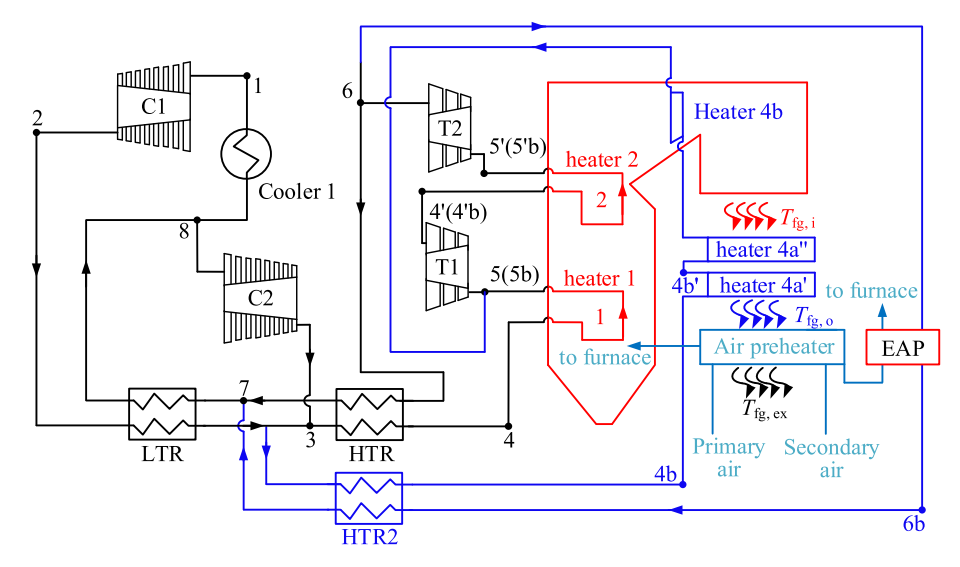


Fig. 1. sCO2 coal fired power plant. The figure is replotted based on Ref. [24].

efficiency increased, reached a maximum, and then decreased with increasing $W_{\rm net}$. This parabolic distribution results from the tradeoff between the decreased efficiency owing to the pressure drops in the heat exchangers and the increased efficiency of the turbomachinery. The maximum thermal efficiency occurred at $W_{\rm net}=300$ and 200 MWe when the PFM and TFM were used, respectively. The above conclusion was drawn with the identical main vapor parameters of 620 °C and 30 MPa.

The magnitude of boiler pressure drop has a decisive influence when system characteristics at various capacities are studied, so it is particularly important to clarify the relationship between boiler pressure drop and power capacity [24,25]. Once the main steam parameters have changed, the cause of the variation in boiler performance is unclear. The limitation is that there is a lack of argumentation about whether it is reasonable to set the main steam parameter to a constant value under various capacities. In practice, the selection of main steam parameters should be adjusted as the capacity changes.

The original contributions are as follows: (1) we will establish a link between the capacity, main steam parameters and thermal efficiency of the sCO2 cycle and compare the results with the findings related to water-steam cycle; (2) for different capacities, the optimum combination of main steam parameters will be given, and a link between capacity values and optimal main steam parameters will be established; (3) The thermal efficiency of the cycle loaded with optimal main steam parameters will be presented as a function of capacity, the effect as well as the mechanism of the optimization will be described in detail. Attention should be paid that all the comprehensive conclusions presented in this paper are predicated on the specified rated operating conditions, for example, when comparing the performance of two distinct units, one with a capacity of "1000 MWe" and the other with "100 MWe", we are explicitly referring to the performance of two separate units, each operating at its designed capacity, but rather assesses a single unit operating under varying loads. The integrated model discussed in this paper was purposely devised to compute the rated operating conditions, with the anticipation that, following modifications, it will also possess the capability to evaluate part-load operating conditions, thus satisfying researches that focus on unit peaking capacity.

The present paper is organized as follows. Section 2.1-2.5 describes the selection of cycles and components as well as specific design details. Section 2.6 describes the characteristics of the integrated model and the principles of its operation. Section 2.7 refers to the validation of models. Section 3 reports the results and discussion. Conclusions are summarized in section 4.

Table 1Equations for components in the cycle [24].

Components	Components Equations and exergy destructions			
• 1				
$\begin{bmatrix} 1 \\ C1 \end{bmatrix}_2$	$\eta_{\text{c,s}} = \frac{h_{2\text{s}} - h_1}{h_2 - h_1}, w_{\text{C1}} = (1 - x_{\text{C2}})(h_2 - h_1); i_{\text{C1}} = w_{\text{C1}} - (1 - x_{\text{C2}})(e_2 - e_1)$			
⁸ C2	$\eta_{\text{c,s}} = \frac{h_{38} - h_8}{h_3 - h_8}, w_{\text{C2}} = x_{\text{C2}}(h_3 - h_8); i_{\text{C2}} = w_{\text{C2}} - x_{\text{C2}}(e_3 - e_8)$			
T1 4'	$\eta_{\mathrm{t,s}} = \frac{h_5 - h_{4'}}{h_5 - h_{4's}}, w_{\mathrm{T1}} = h_5 - h_{4'}; i_{\mathrm{T1}} = e_5 - e_{4'} - w_{\mathrm{T1}}$			
T2 6	$P_{S'} = \sqrt{P_S P_6}, \eta_{t,s} = \frac{h_{S'} - h_6}{h_{S'} - h_{6s}}, w_{T2} = h_{S'} - h_6; i_{T2} = e_{S'} - e_6 - w_{T2}$			
2 8 LTR 7	$T_8 = T_2 + \Delta T_{\rm LTR}, x_{\rm C2} = 1 - \frac{h_7 - h_8}{h_3 - h_2}; i_{\rm LTR} = e_7 - e_8 - (1 - x_{\rm C2})(e_3 - e_2)$			
3 7 HTR 6	$T_7 = T_3 + \Delta T_{\rm HTR}, \ (1-x_{\rm EAP})(h_6-h_7) = (1-x_{\rm Heater~4})(h_4-h_3);$ $i_{\rm HTR} = (1-x_{\rm EAP})(e_6-e_7) - (1-x_{\rm Heater~4})(e_4-e_3)$			
3 4b 7 HTR2 6b	$x_{\text{EAP}}(h_{6\text{b}} - h_7) = x_{\text{Heater 4}}(h_{4\text{b}} - h_3);$ $i_{\text{HTR2}} = x_{\text{EAP}}(e_{6\text{b}} - e_7) - x_{\text{Heater 4}}(e_{4\text{b}} - e_3)$			
8 0 1 Cooler	$i_{\mathrm{Cooler}} = (1-x_{\mathrm{C2}})(e_8-e_1)$			

2. System and components of sCO₂ Brayton cycle

In this part, the features and design guidelines of the cycle system and each component are described in distinct subsections, followed by the computational logic of the integrated model and the accuracy of the component models.

2.1. sCO₂ cycle

For this analysis, we selected the advanced technology-integrated

Table 2Cycle thermal parameters.

Parameters	Value
Net power (<i>W</i> _{net})	100~1000 MWe
Turbine inlet temperature (T_5, T_{5})	620 °C
Turbine T1 inlet pressure (P_5)	30 MPa
Compressor C1 inlet temperature (T_1)	32 °C
Compressor C1 inlet pressure (P_1)	7.6 MPa
Environment temperature (T_0)	20 °C
Pinch temperature at point 4' ($\Delta T_{4'}$)	40 °C
Pinch temperature at point 4b (ΔT_{4b})	30 °C
Cooler pressure drop ($\Delta P_{\rm cooler}$)	0.1 MPa

Table 3Design parameters of components.

Parameters	Value
Primary air temperature entering air preheater	31 °C
Primary air temperature entering furnace	320 °C
Ratio of primary air flow rate to the total air flow rate	0.19
Secondary air temperature entering air preheater	23 °C
Ratio of secondary air flow rate to the total air flow rate	0.81
Excess air coefficient (α)	1.2
Exhaust gas temperature ($T_{fg,ex}$)	123 °C
Ash hopper angle	55°
Flow coefficient of turbine T1 and T2 (ϕ_T)	0.4
Loading coefficient of turbine T1 and T2 (ψ_T)	0.9
Flow coefficient of compressor C1 and C2 (φ_C)	0.33
Loading coefficient of compressor C1 and C2 ($\psi_{\rm C}$)	0.25
Degree of reaction of turbine and compressor (R)	0.5
The number of stages for C1	5
The number of stages for C2	8
Pinch temperature difference in LTR/HTR(ΔT_{LTR} , ΔT_{HTR})	10 °C
Channel type of PCHE	zigzag
Diameter of the channel	2.0 mm
Ratio of the number of hot plates to that of cold plates	2
Width of a PCHE module	0.6 m
Upper limit of the height for a PCHE unit	8.0 m

cycle proposed in Ref. [24], as depicted in Fig. 1. In order to cope with the large pressure drop in the boiler, modular boilers as well as PFM are adopted in the system. Addressing scenarios where flue gas energy struggles to be fully harnessed, the cycle comprises both a top and a bottom cycle. The incorporation of recompression and reheating techniques enhances the efficiency of both the water-steam and supercritical carbon dioxide (sCO₂) cycles [26,27], hence their adoption in both the top and bottom cycles. Intercooling technology has been introduced to alleviate the compressor's workload [28]. The bottom cycle also has an external air preheater (EAP) that recovers excess heat from the bottom cycle into the boiler. However, EAP could not prevent the bottom cycle from being inefficient because of the low heat absorption temperature of the bottom cycle. Therefore, the system also employs overlap energy utilization strategy, which raises the heat absorption temperature of the bottom cycle, thus contributing to the rise in system efficiency [29]. The same heat absorption temperature of the bottom and top cycles contributes to the merging of the two cycles into one, favouring the compactness of the unit.

The performance of the component as a function of thermodynamic parameters is summarized in Table 1, and these parameters can be ascertained utilizing the specified functions. The underlying assumptions include: (i) stable system operation, and (ii) negligible heat loss through the system piping.

The cycle thermal efficiency (η_{th}) is expressed as [24,25].

$$\eta_{\text{th}} = \frac{W_{\text{net}}}{Q_{\text{total}}} = \frac{W_{\text{T1+T2}} - W_{\text{C1+C2}}}{Q_{\text{total}}}$$
(1)

$$Q_{\text{total}} = Q_{\text{Heater 1}} + Q_{\text{Heater 2}} + Q_{\text{Heater 4b}} + Q_{\text{Heater 4a}} + Q_{\text{AP}} - Q_{\text{EAP}}.$$
 (2)

where W_{net} is the net power, that is, the gap between the power

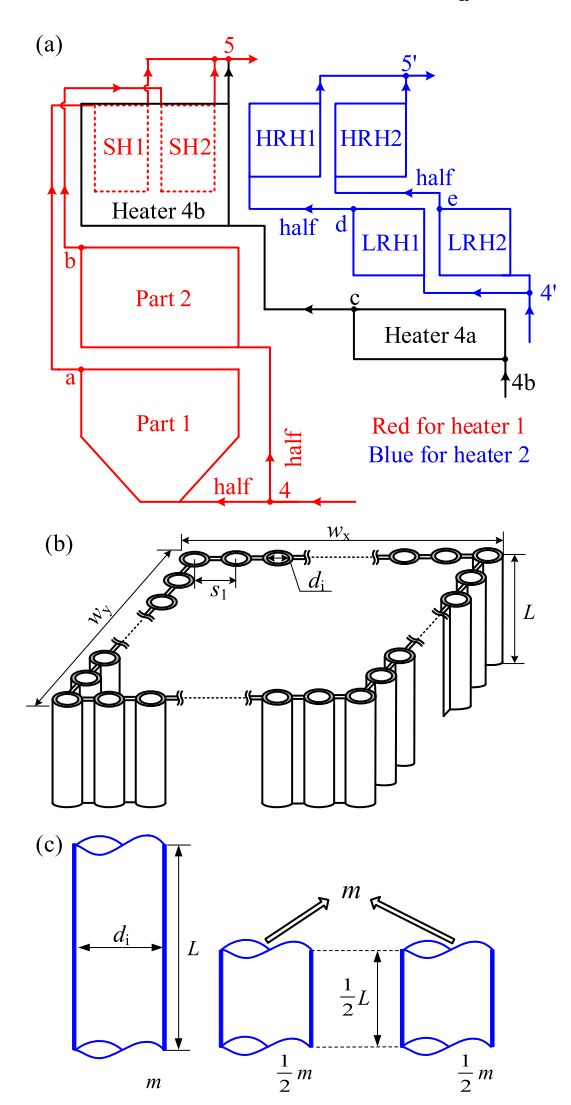


Fig. 2. The partial flow mode (PFM) adapted to the boiler design (This figure is cited from Ref. [24]. Copyright 2020, Elsevier).

generated by the turbine and the power consumed by the compressor; Q is the heat exchange value; and the subscript "total" means the sum value.

The total system loss (I_{total}) is expressed as

$$I_{j} = m_{j}i_{j}, I_{\text{total}} = \sum I_{j}, \tag{3}$$

where i is the specific exergy loss, I is the exergy loss, the subscript j is the component, and j represents the boiler, turbine, etc. The value of $I_{\text{total}}/W_{\text{net}}$ is opposite to the trend of η_{th} , according to ref. [25].

$$\frac{\partial \eta_{\text{th}}}{\partial k} \times \frac{\partial (I_{\text{total}}/W_{\text{net}})}{\partial k} \le 0 \tag{4}$$

2.2. sCO2 boiler

When employed in coal-fired power generation systems, the mass flow rate (m) of the sCO $_2$ cycle surpasses that of the conventional watersteam Rankine cycle by a factor of 6–8, at equivalent capacity levels. This disparity stems from the inherent differences in the cycle characteristics and the distinct physical properties of the working fluids employed. If the boiler's structural configuration remains unaltered, the pressure drop inside it will be very large. In this paper, a π type boiler will be used, Liu [24] proposed a partial flow strategy to form a modular

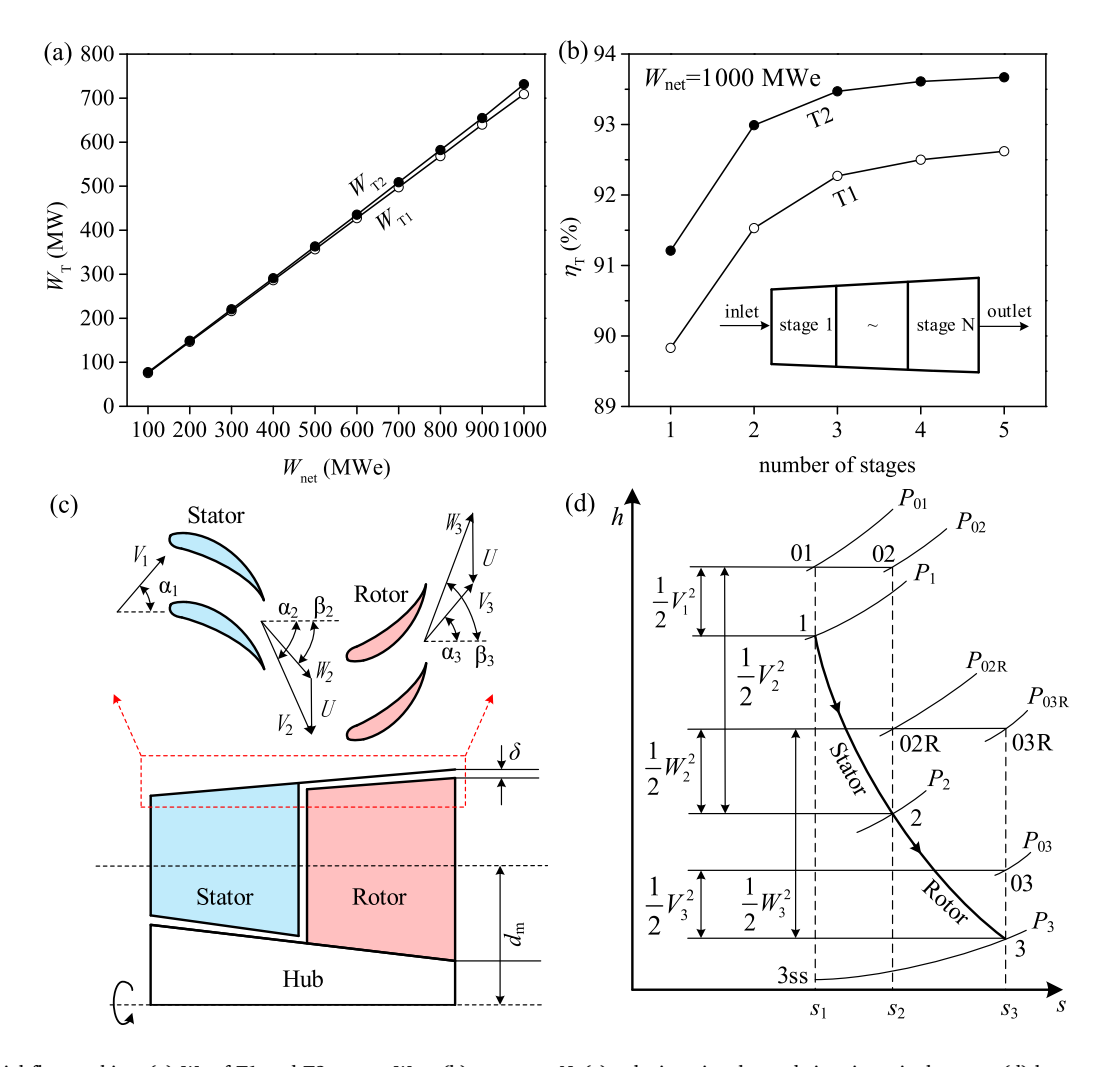


Fig. 3. sCO2 axial flow turbine. (a) W_T of T1 and T2 versus W_{net} . (b) η_T versus N. (c) velocity triangles and sizes in a single stage. (d) h-s curve for sCO2 in the first stage.

design. Adhering to the principles of modular design, the heat exchange surface is segmented into heaters 1, 2, and 4b (Fig. 2a), where the heaters in the furnace chamber belong to the radiant heat transfer surface and the horizontal flue and tail flue heaters belong to the convective heat transfer surface, the cross-sectional structure of the furnace chamber is depicted in Fig. 2b. Sun [30] pointed out that the boiler pressure drop satisfies the relationship $\Delta P \sim m_{\rm pipe}^2 L_{\rm pipe}$ with the flow rate through the pipes m_{pipe} and the pipes length L_{pipe} . Hence, a partial flow model was proposed, which reduces the pressure drop to 1/8 of the original value by dividing the flow rate and the pipe length into two flow lines (see Fig. 2c). After optimization, the pressure drop in the sCO2 boiler has been reduced to a level that is lower than that of a water-steam boiler. However, Liu [24] and Wang [25] have emphasized that the sCO₂ boiler pressure drop still play a barrier to high efficiency of large-capacity plants. A method proposed by Liu [24] will be employed to predict both the structural configuration and pressure drop characteristics of the boiler, ensuring a more comprehensive and accurate analysis. The assumptions for the sCO_2 boiler calculation process are as follows [31]: (i) air or flue gas leaks are disregarded, and (ii) non-uniform heat flux in the furnace width direction is not considered. The pressure drop is.

$$\Delta P = \Delta P_{\rm a} + \Delta P_{\rm f} + \Delta P_{\rm g},\tag{5}$$

where $\Delta P_{\rm a}$, $\Delta P_{\rm f}$, and $\Delta P_{\rm g}$ denote acceleration pressure drop, friction

pressure drop, and gravity pressure drop, respectively, $\Delta P_{\rm a}$ is calculated as

$$\Delta P_{\rm a} = G^2 \left(\frac{1}{\rho_{\rm o}} - \frac{1}{\rho_{\rm i}} \right),\tag{6}$$

where ρ represents the density, G represents the mass flux. When a phase transition occurs, $\Delta P_{\rm a}$ must be taken into account. However, the density variation was limited in the single-phase flow. Hence, $\Delta P_{\rm a}$ occupies a few proportion of the total pressure drop. The determination of $\Delta P_{\rm f}$ and $\Delta P_{\rm g}$ requires the use of integral methods [24]

$$\Delta P_{\rm f} = \int_{\rm whole\ module\ length} \frac{f}{d_{\rm i}} \frac{G^2}{2\rho} dz, \Delta P_{\rm g} = \int_{\rm whole\ module\ length} \rho g dz, \tag{7}$$

where d_i is the pipe internal diameter and g is the gravitational acceleration. The friction factor f is [32].

$$f = \frac{1}{3.24 \lg^2 \left[\left(\frac{\Delta/d_i}{3.7} \right)^{1.11} + \frac{6.9Gd_i}{\mu} \right]},$$
 (8)

where Δ is the roughness of internal tube wall, which is 0.012 mm [33], μ is the viscosity of CO₂.

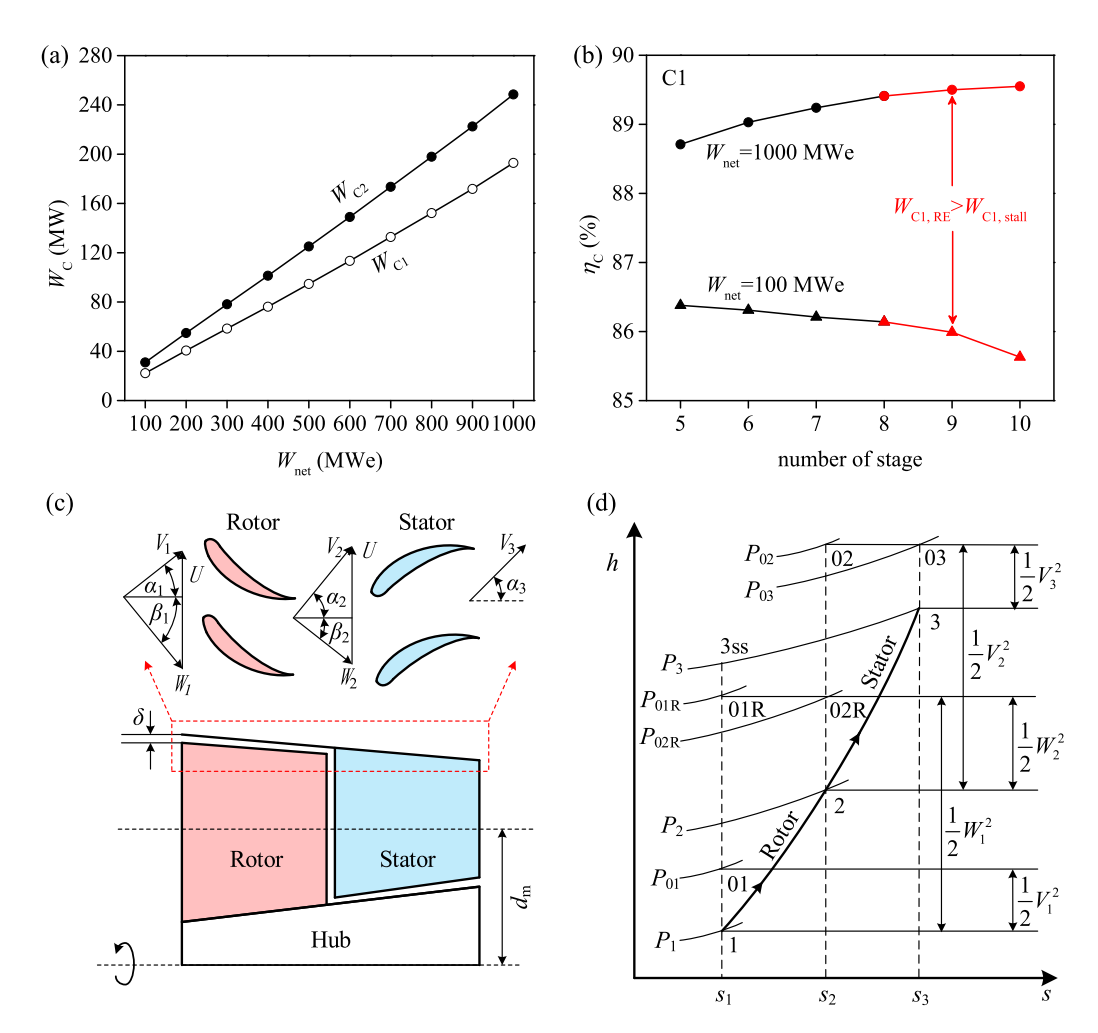


Fig. 4. sCO2 axial flow compressor. (a) W_C of C1 and C2 versus W_{net} . (b) η_C versus N. (c) velocity triangles and sizes in a single stage. (d) h-s curve for sCO2 in the first stage.

2.3. sCO2 turbine

The coal-fired cycle's capacity, spanning an extensive range from 100 to 1000 MWe, presents a formidable challenge to the turbines' power handling capabilities. In the specific instance discussed in this paper, Turbines T1 and T2 have demonstrated their powers by achieving $W_{\rm T1} = 0.702 W_{\rm net}$ and $W_{\rm T2} = 0.725 W_{\rm net}$, respectively, as clearly illustrated in Fig. 3a. For operating conditions characterized by high capacity and a substantial pressure ratio, a multi-stage axial flow turbine is the most suitable choice. As the number of turbine stages (N) increases, the isentropic efficiency (η_T) also rises, consistent with findings in ref. [34]. Given that the efficiency difference between three-stage and four-stage turbines was only 0.25 % (see Fig. 3b), we adopted a three-stage configuration for both T1 and T2. Benefiting from the structure of the axial flow turbine, it is acceptable to ignore the connections between the turbine stages, i.e., the sizes, flow parameters, and thermodynamic parameters of the outlet of one stage and the inlet of the next stage are identical. The illustration in Fig. 3c depicts the size and velocity triangle of a single turbine stage, where sCO₂ sequentially traverses the stator and subsequently the rotor. As sCO₂ flows through the blades, the h-s plots are shown in Fig. 3d, with the inclined solid line representing the actual process and the vertical dashed line indicating the ideal isentropic process. In order to fulfil a satisfactory performance of turbines at various power capacities, the rotating speed (n) was optimized based on the turbine's power [35] as follows:

$$N_{\rm S} = \frac{n\sqrt{Q}}{(h_{\rm i} - h_{\rm o})^{3/4}},\tag{9}$$

where N_S denotes the specific speed, Q is the volume flow rate, and h_i - h_0 is the enthalpy gap across the turbine. It is noteworthy that when $W_T > 450$ MW, n can only adapt to the grid frequency [36].

Multistage turbine is complicated in structure and some assumptions are necessary: (i) dimensionless design parameters flow coefficient (φ_T), loading coefficient (ψ_T) and degree of reaction (R) are constant at each stage, which is set at 0.4, 0.9, and 0.5 [37,38]; (ii) each stage's enthalpy drop is the same [20, 37, 38]. The velocity, flow angle, and mean radius (d_m) shown in Fig. 3c were calculated as follows [20]:

$$U = \sqrt{(h_1 - h_3)/\psi}, V_x = U\phi$$
 (10)

$$\begin{cases} \alpha_2 = \arctan\left(\frac{1-R+\psi/2}{\varphi}\right), \alpha_3 = \arctan\left(\frac{1-R-\psi/2}{\varphi}\right) \\ \beta_2 = \arctan\left(\frac{-R-\psi/2}{\varphi}\right), \beta_3 = \arctan\left(\frac{-R+\psi/2}{\varphi}\right) \end{cases}$$
 (11)

$$d_{\rm m} = \sqrt{\frac{2}{\pi}} \frac{1 + \lambda_1^2}{1 - \lambda_1^2} \frac{m}{\rho_1 V_{\rm X}},\tag{12}$$

where U is the circumferential velocity at the mean radius, V_x is the axial flow velocity, α and β stand for absolute flow angle and relative flow

angle, respectively, subscripts 1, 2 and 3 represent the stator inlet, stator outlet and rotor outlet of a single stage of the turbine. λ is the ratio of hub radius to tip radius.

Upon comparing various loss models [36,39–41], the Aungier model [36] was selected for predicting turbine losses, owing to its suitability for the purpose. The losses in stator and rotor are calculated as

$$Y_{S,T} = Y_{p,T} + Y_{s,T} + Y_{te,T}, Y_{R,T} = Y_{p,T} + Y_{s,T} + Y_{cl,T} + Y_{te,T},$$
(13)

where subscripts S and R represent the stator and rotor, respectively. Y_p is the profile loss, Y_s is the secondary loss, Y_{cl} is the tip clearance loss, and Y_{te} is the trailing edge loss. The pressures at the outlets of the stator and rotor are calculated as [20, 37, 38]

$$P_2 = P_{02} - \frac{P_{01} - P_{02}}{Y_{c.T}} \tag{14}$$

$$P_3 = P_{03R} - \frac{P_{02R} - P_{03R}}{Y_{RT}},\tag{15}$$

where the subscript 0 represents the stationary state in which all the kinetic energy is converted to pressure energy, and the subscript R represents the state in the rotating frame.

The efficiency of turbine is calculated as

$$\eta_{\rm T} = \frac{h_1 - h_7}{h_1 - h_{7ss}}, h_{7ss} = f(P_7, s_1), \tag{16}$$

where h_{7ss} is the enthalpy at the turbine outlet when the expansion process is isentropic.

2.4. sCO₂ compressor

The compressor's primary function lies in harnessing energy to impart pressure to the working mass, in this case, the power consumption of the compressor satisfies $W_{\rm C1}=0.189W_{\rm net}$ and $W_{\rm C2}=0.241W_{\rm net}$ (Fig. 4a). Given the incapacity of centrifugal compressors to handle this specific range of workloads, the employment of an axial compressor becomes a justified decision. Furthermore, since the operating pressure ratio of the CO₂ compressor approximates 4, it becomes imperative to adopt a multi-stage configuration for the compressor. This is crucial as an insufficient number of stages would not only result in undue blade loading but also pose a heightened risk of compressor stalling. Ref. [34] provides the judgement as

$$W_{RE} < W_{RE}^{\min} \tag{17}$$

$$W_{RE} = \sqrt{\frac{P_{oR} - P_{o}}{P_{iR} - P_{i}}}$$
 (18)

$$W_{RE}^{\min} = \frac{(0.15 + 11t_{\max}/c)(0.25 + 10t_{\max}/c)}{1 + 0.4(\theta\sigma/(2\sin(\theta/2)\cos\gamma))^{0.65}},$$
(19)

where W_{RE} and W_{RE}^{\min} are the equivalent speed ratios and stall speed ratios, respectively, $P_{\rm i}$ and $P_{\rm o}$ represent the compressor inlet and outlet pressures, respectively, $P_{\rm iR}$ and $P_{\rm oR}$ stand for the total pressures in relative coordinates, $t_{\rm max}$ is the maximum blade thickness, c is the chord length, θ is the camber angle, σ is the solidity, and γ is the stagger angle.

Stalling occurs when Eq. (17) is satisfied. Fig. 4b's red curve suggests that stall can be prevented in at least eight stages, corroborating the findings of Liu [42]. Given the N- η T relationship, compressors C1 and C2 are chosen as eight-stage configurations. Compressors and turbines are rotating machines with similarities and differences. Firstly, like the turbine, the speed of the compressor is optimized for its own power capacity. In addition, in the context of the single-stage construction of the compressor, it closely resembles a turbine in appearance yet distinctively features an opposing blade arrangement (see Fig. 4c). Lastly, the thermal processes occurring inside the compressor are the

opposite of those in the turbine, Fig. 4d illustrates the h-s diagram for a single-stage compressor, where the solid line represents the actual compression process and the vertical dashed line indicates the ideal compression process. It is worth noting that the inlet of the main compressor C1 is close to the critical point, making the compressor potentially at risk of condensation, so the dimensionless design parameter was chosen to be slightly larger than the optimal value, the compressor's design parameters are $\varphi_C = 0.33$, $\psi_C = 0.25$, R = 0.5 [43,44].

The underlying logic and assumptions in compressor design closely resemble those employed in turbine design. Following a comparative evaluation of three distinct loss models [45–47], the Aungier loss model [47] emerged as the most fitting choice for the specific conditions under investigation in this study, and was consequently adopted for predicting compressor losses.

The losses in blades are calculated as

$$Y_{S,C} = Y_{p,C}, Y_{R,C} = Y_{p,C} + Y_{cl,C},$$
 (20)

where Y_p is profile loss, and Y_{cl} is clearance loss. The pressure at the outlet of the stator and rotor and the isentropic efficiency of the compressor are [42,47,48].

$$P_{02R} = P_{01R} - Y_{R,C}(P_{01R} - P_1)$$
(21)

$$P_{03} = P_{02} - Y_{SC}(P_{02} - P_2) \tag{22}$$

$$\eta_{\rm C} = \frac{h_{\rm 2N+1,ss} - h_1}{h_{\rm 2N+1} - h_1} \tag{23}$$

We will provide an overarching perspective on the potential condensation issues that merit attention. In the context of sCO2 compressors, particularly the sizable axial compressors, condensation is not only a prevalent phenomenon but also more prone to occur than in centrifugal compressors. Unfortunately, the current industry's approach to accounting for condensation loss remains rather limited in scope, and a comprehensive one-dimensional model tailored specifically for the design of CO₂ compressors has yet to be formulated and proposed. Liu [42] has concluded that the condensation issue in axial compressors is inherent and thus, future research endeavors ought to be directed towards centrifugal compressors. Nonetheless, a viable workaround has been proposed, involving a marginal increase in the design parameters $(\varphi \text{ and } \psi)$ to constrain the inlet flow rate and consequently mitigate condensation. This strategy has been embraced in the present study. Allison [49] comprehensively reviewed numerous studies pertaining to the condensation challenge, positing that under saturated conditions, the nucleation time of sCO2 is shorter than its residence time, thereby typically precluding condensation. Furthermore, as the inlet temperature nears the critical point, uncertainty in the nucleation timing escalates. This perspective aligns with Boyce's [50] conclusion, who argued that elevating the temperature during the compression process serves as an effective means to forestall condensation. Considering the research scope of this paper, while elevating the compressor inlet temperature inevitably results in a modest decline in compressor efficiency, this decrement is negligible and holds paramount significance in averting condensation. Consequently, we contend that maintaining the inlet temperature in close proximity to the critical point is unwarranted. Moving forward, we aspire to refine our one-dimensional model by incorporating condensation losses into its calculations.

2.5. sCO₂ recuperators

A printed circuit plate heat exchanger (PCHE) is the optimal choice for heat recovery because of its exceptional heat transfer capabilities and compact design [51]. However, the heat load capacity of the PCHE is inherently constrained by manufacturing constraints, as outlined in ref. [52]. To optimize heat recovery efficiency, the adoption of a parallel pipe network configuration becomes imperative. For either side of the

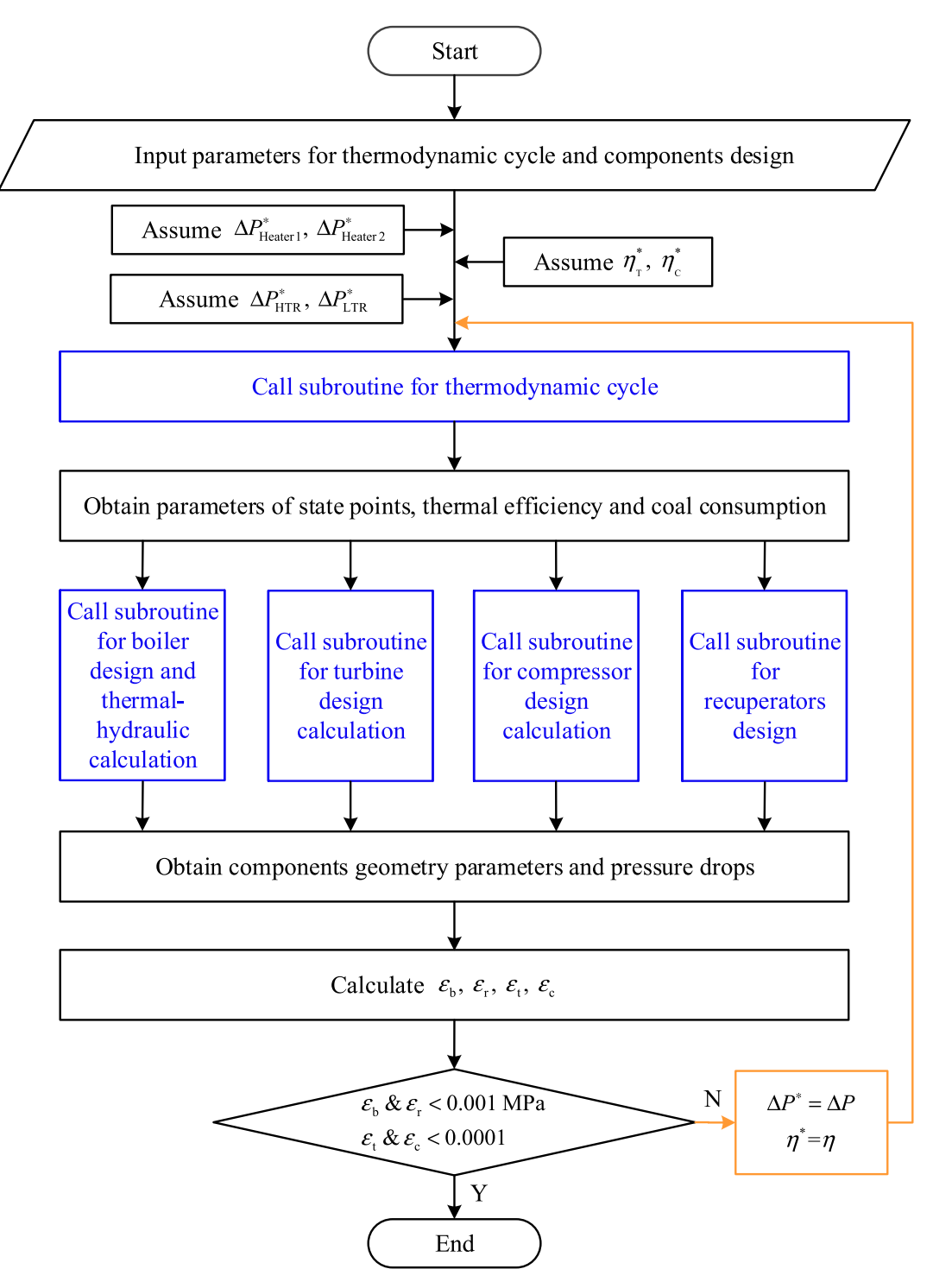


Fig. 5. The calculation process.

recuperator, the inlet mass flow is first diverted into the pipes; in turn, the work mass in each pipe is diverted into the parallel PCHEs. In the present study, we have opted for a zigzag channel configuration featuring a semicircular cross-sectional profile for the PCHE. This design has been extensively validated to demonstrate superior performance in flow heat transfer processes, thereby significantly enhancing the overall heat recovery efficiency [53]. Delineating the pressure drop and heat transfer capabilities of the heat exchangers is paramount for an accurate assessment of cycle efficiency. Consequently, we called a simulation model to meticulously calculate the performance metrics of each individual heat exchanger, encompassing the HTR, HTR2, and LTR.

The assumptions used in the parallel pipe network and PCHE models are: (i) the mass flow is equally distributed within pipes. (ii) the mass flow rate is distributed according to the same pressure drop in each branch when the mass flows from the pipe to PCHEs. (iii) due to the horizontal arrangement of the PCHE, the overall height of the recuperators is small and the gravity pressure drop is ignored, (iv) there is no leakage of the work mass and no heat loss from the pipeline during the process [52–54]. According to the assumption conditions can be solved for the branch work mass flow distribution and flow resistance characteristics, the pressure drop solution process is too cumbersome, please see ref. [55].

Table 4
The accuracy of models.

Case	Item	Value of Ref	Result/error
Case1 [24] Boiler (1000	Pressure drops in Heater 1 (MPa)	1.99	2.02/1.51 %
MWe)	Pressure drops in Heater 2 (MPa)	0.44	0.45/2.22 %
Case2 [54] Turbine	Isentropic efficiency (%)	91.60	93.85/2.45 %
Case3 [34] Compressor	Isentropic efficiency (%)	91.63	91.05/0.63 %
	Average radius (mm)	274.57	278.59/1.45 %
Case4 [51]	Length (m)	0.86	0.87/1.16 %
Recuperator	Pressure drop of cold side (MPa)	1.40	1.41/0.71 %
	Pressure drop of hot side (MPa)	1.08	1.09/0.93 %

2.6. The computational logic of the integrated model

The model involved in this paper is compiled based on MATLAB software, and the physical properties of the work material are taken from the software REFPROP 9.1 from NIST, the mixing exergy losses are neglected in this paper, assuming that the fluids have the same pressure and temperature prior to mixing at the nodes. The calculation process is outlined in Fig. 5 as follows:

(i) Tables 2 and 3 show the thermal parameters of the cycle and the design parameters of the components, which are set as initial parameters; (ii) assuming component performance for the system, including the boiler and recuperators pressure drops $(\Delta P_{\text{boiler}} \text{ and } \Delta P_{\text{HTR} + \text{LTR} + \text{HTR2}})$, as well as the η_{T} and η_{C} ; (iii) invoking the thermodynamic cycle program to calculate the thermodynamic parameters at various points within the cycle, as well as m and energy values of the components, leveraging the equations presented in Table 1 alongside the prescribed initial parameters; (iv) based on the parameters obtained in step (iii), the component modelling subroutines are invoked to calculate the new component performances respectively, including ΔP_{boiler} , $\Delta P_{\text{HTR}\ +\ \text{LTR}\ +\ \text{HTR2}}$, η_{T} and η_{C} ; (v) the component performance calculated in step (iv) is compared with the component performance assumed in step (ii), and the procedure is recognised as converged when the error in ΔP_{boiler} and ΔP_{HTR} + LTR + HTR2 satisfies $\varepsilon_{\rm b}$ & $\varepsilon_{\rm r}{<}0.001$ MPa, and also the error in $\eta_{\rm T}$ and $\eta_{\rm C}$ meets ε_t & ε_c <0.0001. If the result of either component performance calculation does not satisfy the convergence condition, the component performance mentioned in step (ii) is replaced by the component performance calculated in (iv) and steps (ii)~(v) are re-executed until convergence is satisfied.

A brief explanation will be given as to how the integrated model can be utilized for the purpose of this paper. Firstly, η_{th} can be calculated after the convergence of the above procedure (Eq. (1)). As for how to obtain η_{th} under various operating conditions, we change the W_{net} , T_5 or P_5 in Table 2 individually, and give the updated Table 2 to the step (i) for calculation. This paper also deals with the optimization search, however, there is only two optimization parameters T_5 , P_5 (which can even be regarded as one) and one optimization objective (η_{th}) at each W_{net} case, so, instead of using an optimization algorithm, all operating conditions are computed and optimal values are selected manually.

The correlations and equations presented in this paper are specifically tailored for air as the working medium, yet their versatility extends beyond this realm. Notably, these equations have been successfully employed in relevant studies [20,24,34,48] focusing on components of sCO₂ cycle, showcasing their applicability across diverse

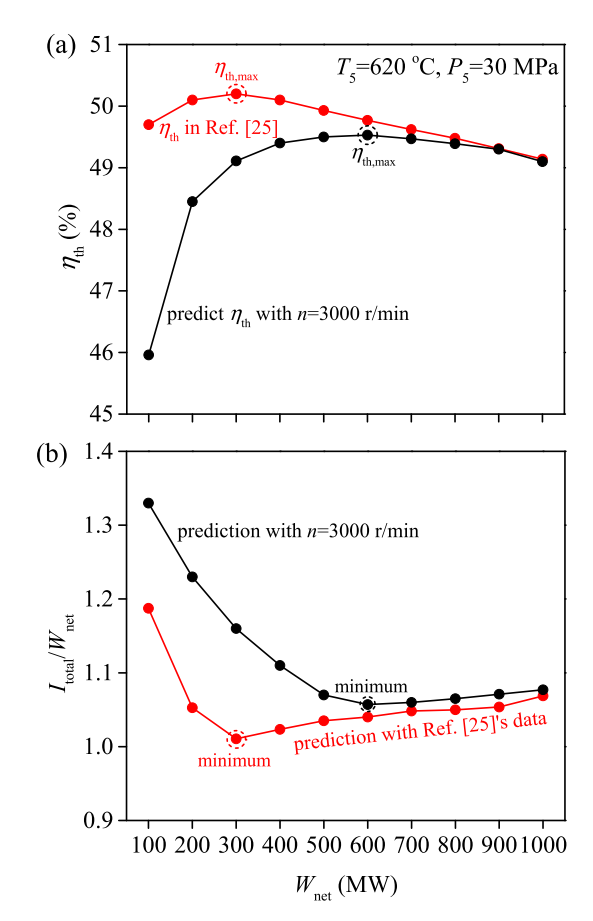


Fig. 6. Predicted η_{th} and I_{total}/W_{net} with n=3000 r/min and ref. [25]'s data.

fluid systems. Furthermore, the validation cases conducted in this research, leveraging sCO_2 as the working fluid, reveal minimal discrepancies between the calculated and reference values, thereby reinforcing the equations' validity and robustness for sCO_2 -based applications.

2.7. The accuracy of models

In order to prevent bias in the results due to low model accuracy, component simulation models were validated with cases. The results are summarized in Table 4.

Case 1 [24] contains boiler characteristics and the boiler pressure drop $\Delta P_{\rm boiler}$ at the capacity of 1000 MWe were selected for comparison. The results in this paper are 1.99 MPa and 0.44 MPa for heater 1 and heater 2, respectively, which are similar to the 2.02 MPa and 0.45 MPa in reference.

Case 2 [56] demonstrates a three-stage axial flow turbine with a turbine efficiency $\eta_{\rm T}$ of 93.8 %, which is calculated to be 92.2 % in this paper.

Case 3 [34] shows an axial compressor with a mean-line model, that is, the hub radius plus half of the blade height was the same for all stages. The isentropic efficiency $\eta_{C}=91.63$ % and the mean radius $d_{m}=274.57$ mm. The calculations in this paper result in $\eta_{C}=91.05$ % and $d_{m}=278.59$ mm.

Case 4 [53] presents the PCHE in a system with a power capacity of 10 MWe. The unit length $L_{\rm z}$ is 0.86 m, and the pressure drops at the cold and hot sides $\Delta P_{\rm C}$ and $\Delta P_{\rm h}$ are 1.40 MPa and 1.08 MPa, respectively. In this paper, the $L_{\rm z}$ is calculated to be 0.87 m, $\Delta P_{\rm C}$ and $\Delta P_{\rm h}$ are 1.41 MPa and 1.09 MPa, respectively.

The relative errors shown in Table 4 indicate that the accuracy of the component models is acceptable, ensuring that the conclusions of this

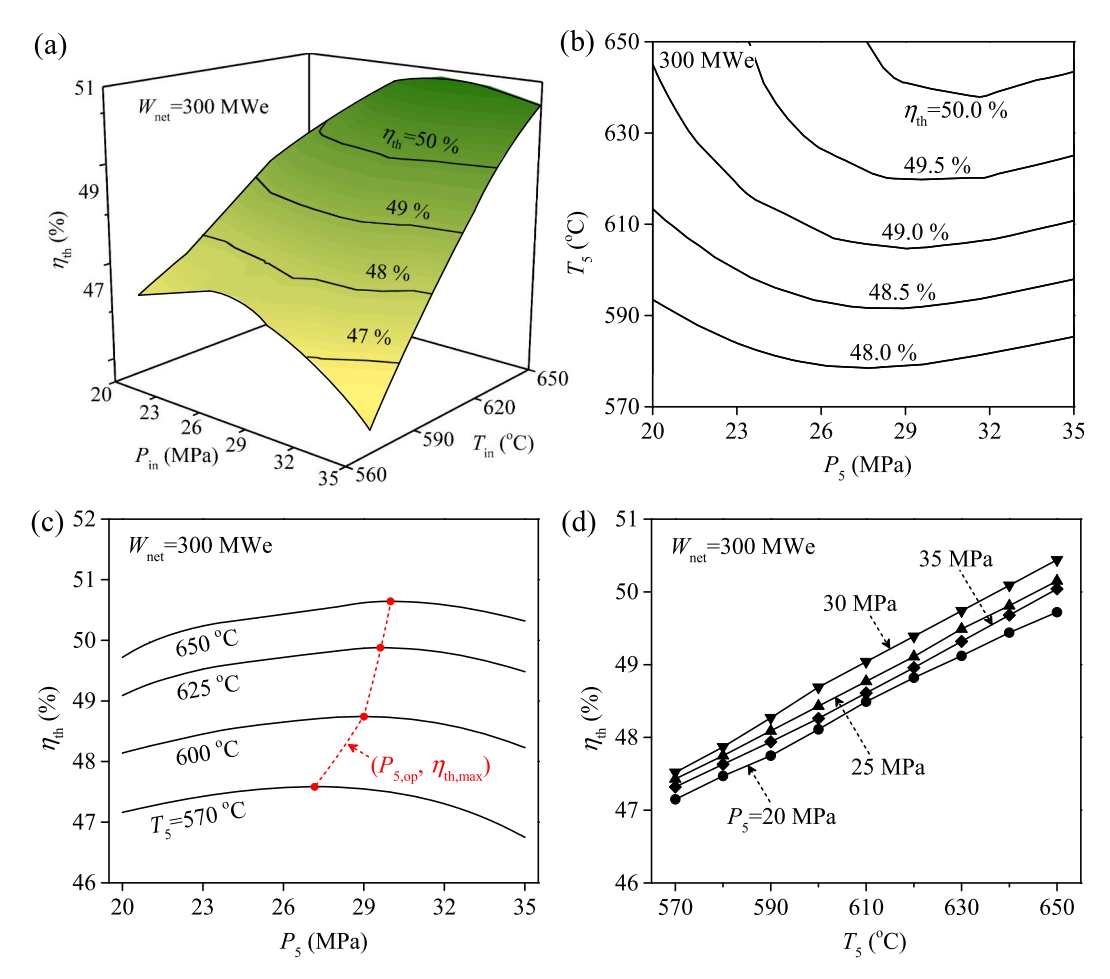


Fig. 7. (a) Surface diagram of P_5 , T_5 versus η_{th} relation. (b) plan of P_5 , T_5 versus η_{th} relation. (c) P_5 versus η_{th} relation. (d) T_5 versus η_{th} relation.

paper are plausible. Further, we validated the integrated model by evaluating its predictive accuracy and correlating $I_{\rm total}$ with the cycle performance. Wang [25] observed a parabolic relationship between $\eta_{\rm th}$ and $W_{\rm net}$, peaking at $W_{\rm net}=300$ MWe. Upon comparing our thermal efficiency curves with the original data, we have confirmed a negligible peak deviation of merely 0.6 %, thereby validating the precision of our model. Additionally, taking into account both speed and grid frequency compatibility, a rotational speed of 3000 r/min emerges as a viable alternative [36]. For the case of n=3000 r/min, $\eta_{\rm th}$ exhibits a similar parabolic trend with $W_{\rm net}$, peaking at $W_{\rm net}=600$ MWe (Fig. 6a). Additionally, $I_{\rm total}/W_{\rm net}$ exhibited a parabolic trend with $W_{\rm net}$, reaching a minimum at $W_{\rm net}=300$ and 600 MWe (Fig. 6b). This validates the correlation between the exergy loss and cycle performance.

3. Results and discussion

The correlation between $\eta_{\rm th}$ and the primary steam parameters, under the condition of $W_{\rm net}=300$ MWe, is illustrated in Fig. 7a and b $\eta_{\rm th}$ exhibits a parabolic trend with P_5 (see Fig. 7c), while monotonically increasing with T_5 (see Fig. 7d). Specifically, for $W_{\rm net}=300$ MWe, the optimal combination of main steam parameters is $T_5=650\,^{\circ}{\rm C}$, $P_5=30$ MPa. We point out that within the capacity range of 100–1000 MWe, there exist optimal configurations of the main steam parameters for cycles. Elucidating these principles is crucial for gaining insights into the mechanisms underpinning the optimization of cyclic system performance. Subsequently, we will explore the relationship between $\eta_{\rm th}$ and variables such as P_5 and T_5 based on constant capacity conditions, considering component performance, exergy losses, and other relevant factors.

Fig. 7 outlines the impacts of main steam pressure and temperature on the system's performance, prompting the question of whether these parameters solely dictate the system's efficacy. Notably, the system is influenced by a myriad of parameters, with main steam characteristics constituting merely a subset. In this context, we concisely introduce a select few factors to facilitate users in gaining a preliminary understanding of the relative influence each exerts on the system's behavior.

The boiler in this research adopts the PFM strategy, specifically designed to minimize $\Delta P_{\mathrm{boiler}}$. Liu [24] and Sun [30] have emphatically stated that the configuration of the boiler for the sCO₂ coal-fired cycle should not merely replicate that of water steam cycle boilers. However, their system models, which solely encompassed the boiler, yielded conclusions with limited scope and persuasiveness. Alternatively, we called an integrated model to attain more precise results, while also elucidating the impact of PFM versus the Total Flow Model (TFM) on the system's performance. As evident in Fig. 8a, which compares $\Delta P_{\mathrm{boiler}}$ against W_{net} for both flow models, the pressure drop associated with TFM is approximately an order of magnitude higher than that of PFM. This substantial increase in additional pressure demanded by the compressor subsequently elevates its workload, ultimately leading to a decrease in η_{th} , as illustrated in Fig. 8b.

The disparities arising from distinct boiler operation strategies underscore the profound influence that component structural modifications can exert on system performance. Notably, even for pre-designed components with fixed structures, the adoption of varying operational strategies can still significantly alter system performance. In contrast to the strategy which fixed n at 3000 r/min to accommodate grid requirements and mitigate potential gearbox losses, we assign optimal speeds tailored to different rated capacities [34,35]. As depicted in

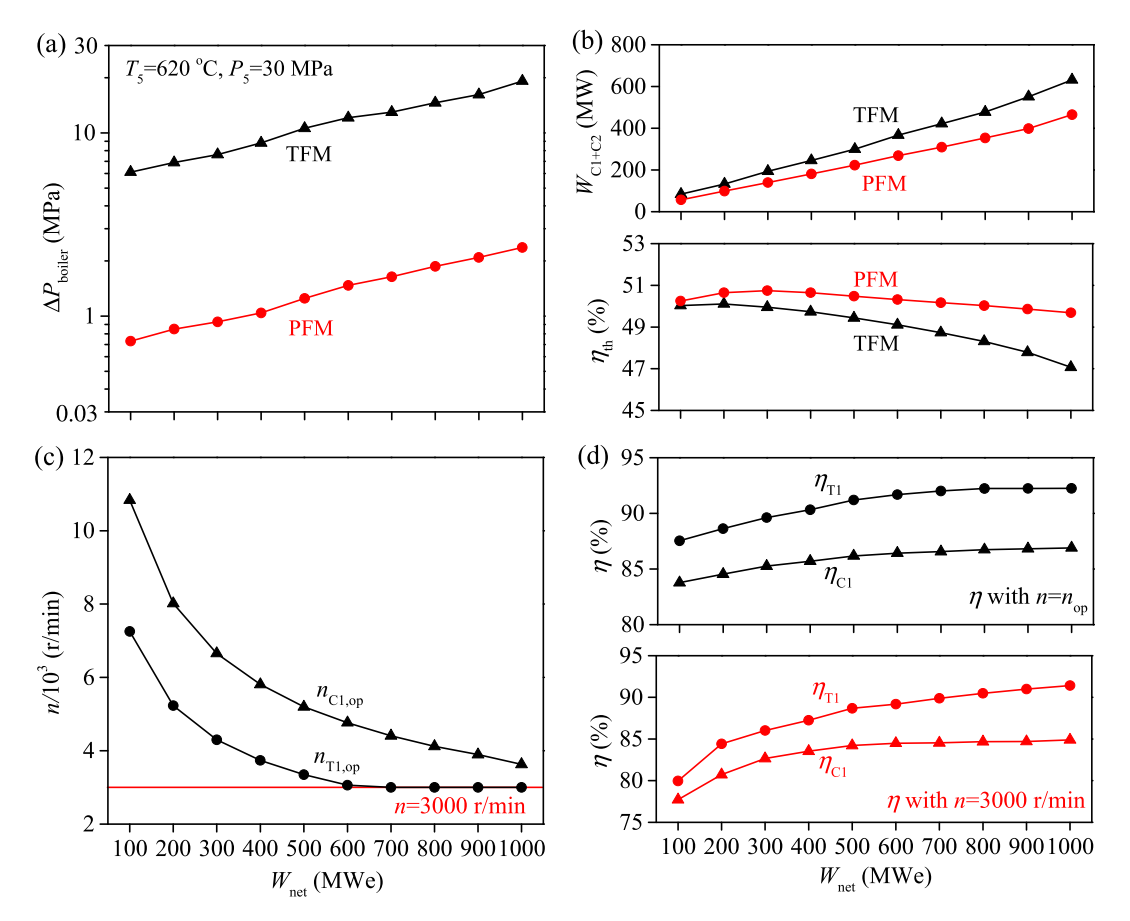


Fig. 8. Impact of component operation strategy on components and system. (a) boiler pressure drop. (b) W_C and η_{th} . (c) rotation speed. (d) turbomachinery efficiencies.

Fig. 8c, the lowermost straight line represents the minimum feasible rotational speed, whereas the upper curve signifies the recommended speed for optimal $\eta_{\rm T}$ and $\eta_{\rm C}$, with the intermediate space constituting the desirable operational range. It is evident that there exists a substantial disparity in turbomachinery efficiencies between these two rotational speed scenarios (refer to Fig. 8d). This efficiency gap primarily stems from the reduced ability of the internal mainstream to withstand perturbations at lower speeds, which enhances irreversible losses during pressure fluctuations in sCO₂, thereby compromising the power generation capacity. When dealing with high-capacity units, component limitations necessitate adhering to n of 3000 r/min. Conversely, for small-capacity units, adjusting n to 3000 r/min is discouraged as it would markedly diminish $\eta_{\rm th}$.

In the following, the relationship between the main steam parameters and the thermal efficiency of the system will be analyzed in detail, while the mechanism by which other factors affect the system performance can also be derived along the following lines.

3.1. Effect of P5 on cycle efficiency

As P_5 escalates, the net specific work of the system ($w_{\rm net}$) undergoes an initial swift augmentation due to the widening enthalpy gap. Subsequently, the pace of the increase trend becomes gentle, giving rise to an initial steep reduction in m, which subsequently plateaus (refer to Fig. 9a). Pressure drop of components exhibit consistent trends with m (see Fig. 9b), benefiting the system by alleviating the compressor load. It is imperative to recognize that elevating P_5 introduces potential stresses to the system. Firstly, the escalation of P_5 triggers a decline in both $\eta_{\rm T}$ and $\eta_{\rm C}$, attributable to the intensified losses occurring at the tip clearance. Secondly, achieving a higher P_5 necessitates the compressor to supply additional pressure, placing further demands on the system. The

interplay between these two opposing effects cause the subsequent phenomenon: As P_5 initially increased from 20 MPa, W_C and Q_{boiler} decreased owing to the rapid decrease in m (Fig. 9c), indicating that the negative effects were less significant at low P_5 . However, once P_5 exceeds 30 MPa (for $W_{\text{net}} = 300$ MWe), the attenuation in the rate of decrease of m exacerbates the impact of P_5 augmentation on $W_{\mathbb{C}}$ and Qboiler, rendering it more pronounced, which harms the system performance. In conclusion, the increase of P_5 had a multifaceted influence on the system's overall performance. Fig. 4 in ref. [21] notes that with an increase in the compressor pressure ratio, the hydrodynamic force and power capacity of the turbine increase monotonically. However, as the pressure ratio rise to larger values, the increment in W_C approached that of the W_T 's, resulting in the η_{th} tends to increase and then decrease. We observe that the W_T and W_C in ref. [21] exhibit a monotonic increase, contrasting with the findings presented in this study. This discrepancy arises from the fact that previous research has predominantly concentrated on fixed-flow conditions, whereas our analysis expands the investigation to encompass fixed-capacity conditions.

The conclusions could be further supported. The relationships among exergy losses and P_5 are shown in Fig. 9d. $I_{\rm total}$ exhibits a parabolic trend with increasing P_5 , culminating in a minimum at $P_5=30$ MPa. This downward trend is primarily attributed to reduction in $I_{\rm boiler}$, whereas the subsequent upward trend is predominantly driven by increases in $I_{\rm T1+T2}$ and $I_{\rm C1+C2}$. This parabolic distribution underscores the intricate interplay between parameters, where a reduction in m partially alleviates exergy losses, yet simultaneously, the escalating compressor load becomes dominant, triggering a surge in $I_{\rm total}$ that ultimately undermines the system's overall performance. In Fig. 9d, $I_{\rm C1+C2}$ also exhibit a parabolic shape, which results from a trade-off of several factors. Between P_5 values of 20 MPa and 23 MPa, there is a marked decrease in m, constituting the primary factor contributing to the

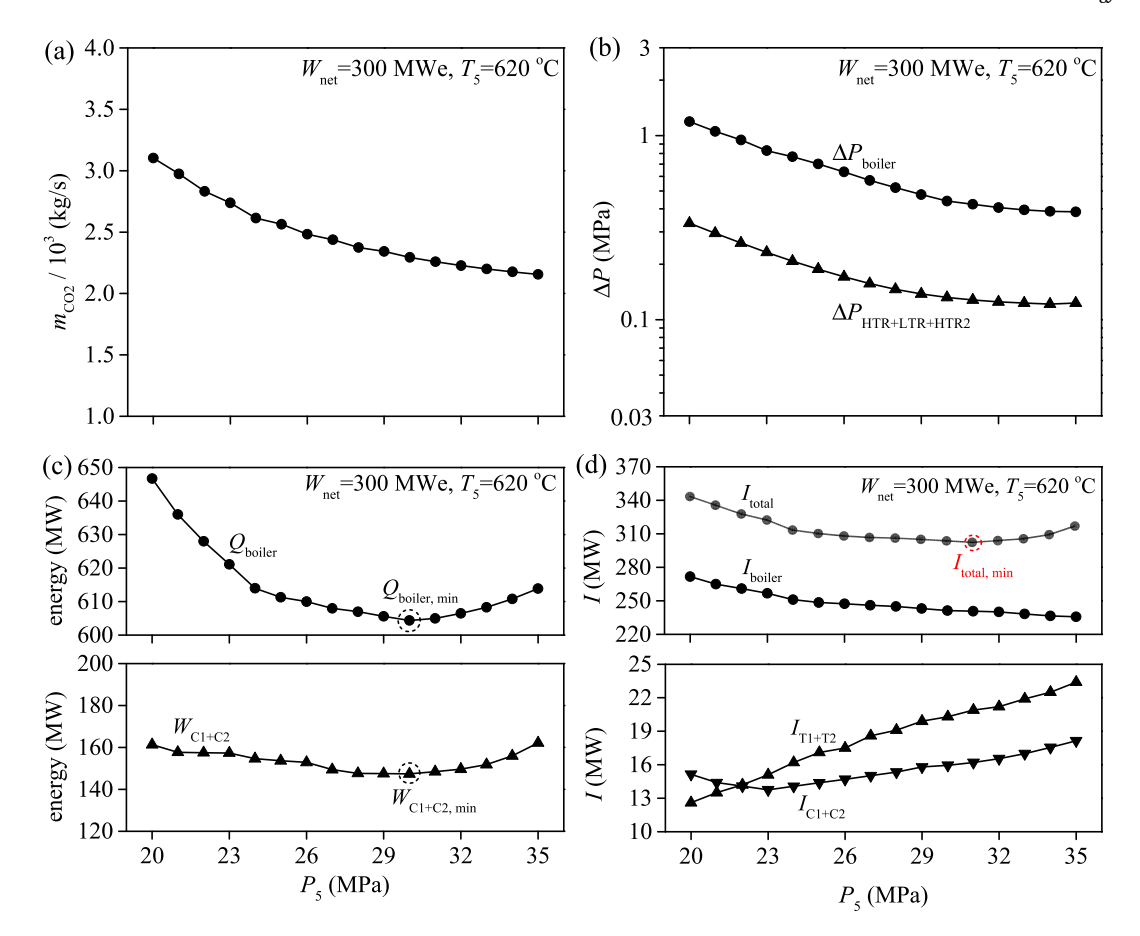


Fig. 9. (a) m_{CO2} versus P_5 relation. (b) pressure drop versus P_5 relation. (c) energy terms versus P_5 relation. (d) exergy losses versus P_5 relation.

reduction in $I_{\rm C1+C2}$. Whereas, between P_5 at 23 MPa and 35 MPa, $I_{\rm C1+C2}$ starts to turn up due to the combined effect of a more gentle trend in m-curve and the increased workload of the compressor. Fig. 6 in ref. [57] illustrates the trend of increasing and then decreasing of the system's exergy efficiency ($\eta_{\rm ex}$) with increasing turbine inlet pressure, the increase of $\eta_{\rm ex}$ is due to the decrease of the exergy loss of the steam generator, and $\eta_{\rm ex}$ turns to decrease because of the increase of turbine and pump's exergy losses, which is a similar conclusion to that of this paper.

We conclude that η_{th} exhibits a parabolic trend with increasing P_5 , resulting from a trade-off between positive and negative effects: an increase in boiler's performance and a decrease in turbomachinery's performance, respectively. When the positive and negative effects are equal, P_5 reaches the optimal point, at which the system's thermal efficiency attains its peak value. As for a case with $W_{\text{net}} = 300$ MWe, the optimal pressure is 30 MPa. Subsequently, the optimal main steam pressure is denoted as $P_{5,\mathrm{op}}$. We believe that an excessively high P_5 is detrimental to the system's performance, primarily stemming from the augmented compressor load. This observation aligns with the idea presented in ref. [58], which contends that in a water-steam cycle, excessively high main steam pressure exacerbates turbine losses, thereby reducing system efficiency. This underscores a consensus that an excessive main steam pressure is detrimental cycle system. In this section, the relationship between system performance and component's pressure drop, efficiency, and exergy loss are established, which of them help to understand the comprehensive impact of P_5 on the system.

3.2. Effect of T₅ on cycle efficiency

As depicted in Fig. 10a, m exhibits a consistent downward trend with increasing T_5 , primarily because of the enlarged enthalpy gap within the

turbine. Component's performance varies accordingly: ΔP_{boiler} and $\Delta P_{\rm HTR~+~LTR~+~HTR2}$ decrease with m (see Fig. 10b), favoring system efficiency. Moreover, W_C shows a decreasing trend (Fig. 10c) due to the combined effect of the enthalpy gap, m and η_C , positively affecting the system performance. The graph depicted in Fig. 3 of ref. [21] illustrates the impact of elevating the maximum cycle temperature on the cycle performance under fixed-flow operating conditions. Notably, both the turbine's output work and the overall heat input exhibit an upward trend, with the turbine's output work demonstrating a more pronounced increase. Consequently, this results in a sustained augmentation of the net output work and cycle efficiency. Despite the distinction between fixed-flow and fixed-capacity conditions, both scenarios yield a congruent correlation between the main steam temperature and the thermal efficiency η_{th} . Ref. [15] depicts the distribution of the η_{th} as the main vapor temperature increases in water-steam cycle, where the η_{th} rises uniformly, demonstrating that the selection strategies of water-steam cycle and sCO2 cycle are the same when it comes to main steam temperature.

The relationship between exergy losses and T_5 is shown in Fig. 10d. Significantly, the exergy losses in all components excluding the turbine exhibit a decreasing trend with the increase in T_5 , primarily stemming from the reduction in m. Conversely, I_{T1+T2} displays an upward trend, which can be attributed to the notable decrease in η_T . As only I_{T1+T2} increases, and that is significantly less than the combined decrease in the exergy losses of the other components, I_{total} shows an overall decreasing trend. In prior turbine related research [20], it highlighted the paradoxical effect of increasing T_5 ; while it adversely impacts turbine performance, it benefits the overall cycle performance. We have now satisfactorily addressed this inquiry, elevating T_5 has an adverse impact on the turbine's performance, albeit this deterioration is insignificant when juxtaposed against the substantial benefits accrued by the

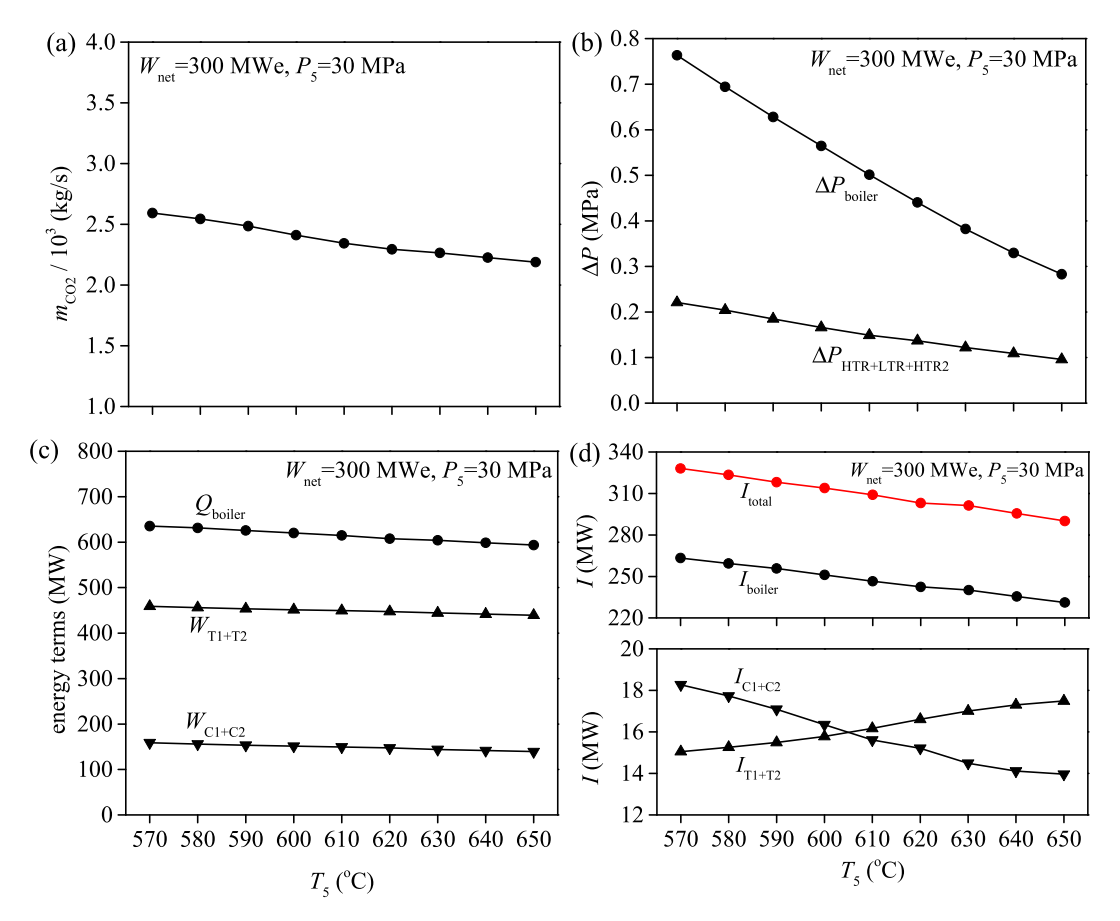


Fig. 10. (a) m_{CO2} versus T_5 relation. (b) pressure drop versus T_5 relation. (c) energy terms versus T_5 relation. (d) exergy losses versus T_5 relation.

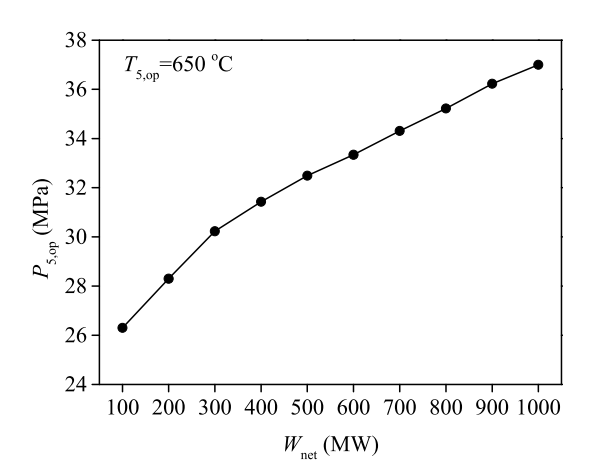


Fig. 11. $T_{5,op}$ and $P_{5,op}$ for various capacities.

remaining components.

With respect to the influence of T_5 on cycle performance, refs. [21–32,56–59] consistently presents analogous observations. Our analysis concludes that under both fixed-capacity and fixed-flow conditions, an augmentation in T_5 enhance cycle efficiency, albeit through disparate mechanisms. Importantly, our research underscores the need for caution against excessively elevated T_5 levels, not solely due to the piping's maximum tolerable temperature limits but also because of its detrimental effect on $\eta_{\rm T}$.

3.3. Optimal T_5 , P_5 for various W_{net}

In this section, we consolidate the preceding analyses and derive additional insights pertinent to the comprehensive capacity spectrum spanning from 100 to 1000 MWe. Fig. 11 showcases the optimal combinations of main steam parameters tailored to distinct capacity scenarios. Notably, T_{5,op} remains consistent at 650 °C across the entire spectrum of W_{net} values, underscoring the persistent positive correlation between η_{th} and T_5 across this comprehensive capacity range. For another main steam parameter, $P_{5,op}$, increased monotonically from 26 to 37 MPa as W_{net} increased. This trend results primarily from the varying trade-offs between the positive and negative effects across different capacities. For high-capacity systems, η_T is higher [20] and less sensitive to P_5 , leading to a more pronounced increase in w_{net} with increasing P_5 . Concurrently, the reduction in m became more evident as P_5 increased. Fig. 12a and b demonstrate that ΔP_{boiler} and I_{boiler} exhibit a similar trend to m, indicating that the positive impact of increased P_5 on the system becomes more pronounced. On the other hand, the negative impact of increased P_5 on the system also varies across capacities. Fig. 12c further illustrates a pronounced increase in the slope of I_{C1+C2} as capacity escalates. Nonetheless, when juxtaposed with Iboiler, both the initial value and the rate of change in I_{C1+C2} exhibit more subdued variations (analogous to those observed in the turbine), indicative of a relatively stable, persistent negative influence of the elevation in P_5 on the overall system performance. As the positive effect intensified while the negative effect remained steady, the parabolic peak shifted to the right (Fig. 12d), explaining the increase in $P_{5,op}$ with W_{net} . Importantly, the $P_{5,op}$ values reported for high-capacity units in this study potentially surpass the current operational limits of contemporary units. Therefore, the findings presented herein should be regarded as aspirational benchmarks, and the practical optimization targets ought to account for

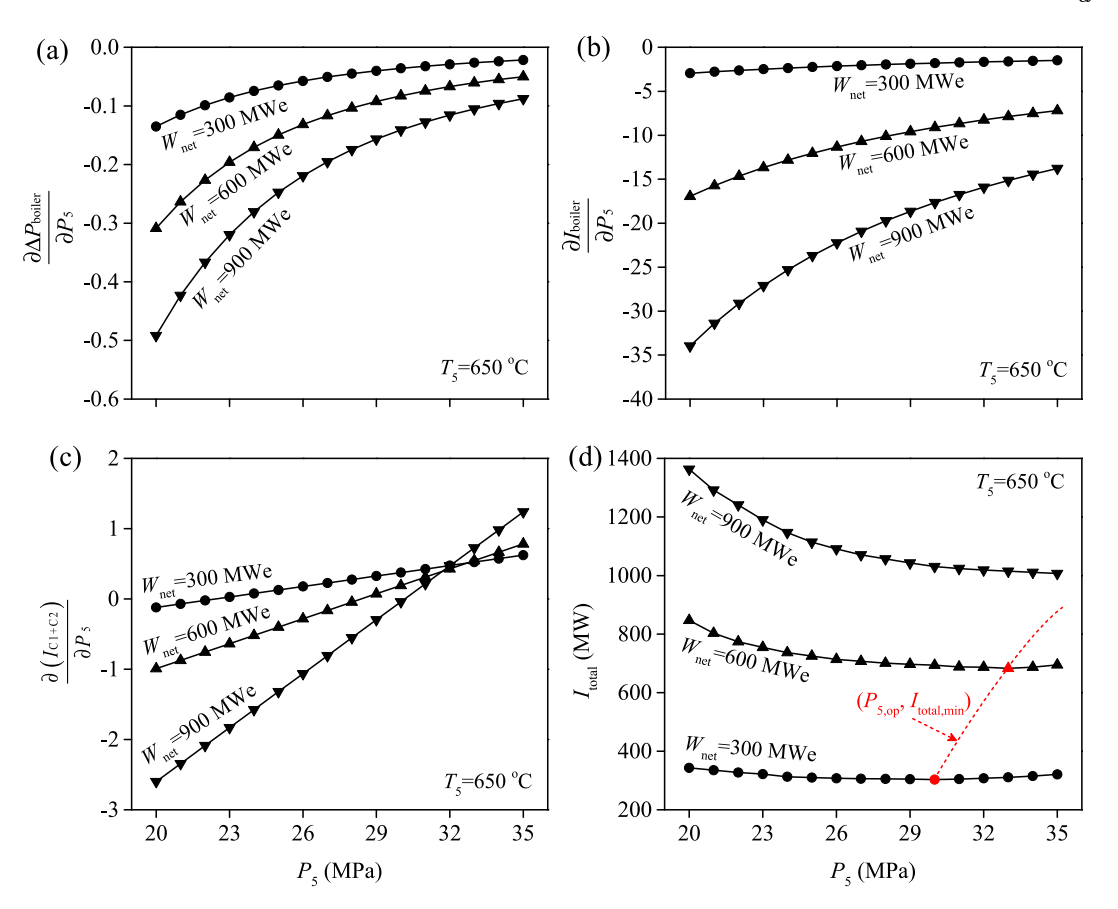


Fig. 12. The reason that $P_{5,\text{op}}$ increases with W_{net} . (a) boiler pressure drop slope. (b) boiler exergy loss slope. (c) compressor exergy loss slope. (d) total exergy loss versus P_5 at various capacities.

the specific unit's maximum tolerable P₅ threshold.

As depicted in Fig. 9 of ref. [60], the influence of the maximum cycle temperature on the optimal cycle pressure ratio is elucidated. This effect stems from a multifaceted interplay of factors, including turbine output work, the recuperators' heat transfer capabilities, and the heat absorption temperature. In particular, a monotonically increasing trend is observed in the optimal cycle pressure ratio as the maximum cycle temperature escalates. Our conclusions complement well the relationship between the optimal cycle pressure ratio and power capacity. Ref. [21] optimized key parameters, including T_5 , compressor pressure ratio, and split ratio under fixed-flow conditions. Notably, the T_5 was optimized from an initial 550 °C-750 °C, while the compressor pressure ratio was optimized from 2.60 to nearly 5.75. With regard to the main steam pressure, the optimization trend is found to be diametrically opposed to the recommendations proffered in this paper. Notably, it becomes apparent that the conclusions formulated under fixed-flow conditions diverge from those derived from constant capacity conditions. In this section, we summarize $T_{5,\mathrm{op}}$ and $P_{5,\mathrm{op}}$ for the distinct capacity cases. $T_{5,op}$ remained constant across the varying W_{net} values, whereas $P_{5,op}$ exhibited a monotonic increase with W_{net} . Subsequently, we shall employ these optimized main steam parameters to replace the initial values of 620 $^{\circ}\text{C}$ and 30 MPa. This endeavor facilitated the development of a revised thermal efficiency curve, enabling us to comprehensively evaluate the performance disparities that arose before and subsequent to the optimization of the main steam conditions.

3.4. Maximum η_{th} at various W_{net}

Fig. 13a illustrates a monotonic increase in the $\eta_{th,max}$ of the cycle as a function of W_{net} . This observed trend stems primarily from an intricate interplay of both positive and negative effects. To elucidate the

relationship between these opposing influences within the cycle as W_{net} changes, we analyse a specific condition characterized by constant main steam parameters. Following this, we undertake a comparative of the shifts in these effects, both prior to and subsequent to the optimization process. Increasing W_{net} with fixed main steam parameters leads to a significant negative effect from increased ΔP_{boiler} and a positive effect from increased η_T and η_C . When W_{net} increases from 100 MWe, the positive effect is greater than the negative effect and η_{th} rises. As W_{net} continues to increase, the rising trends of η_T and η_C become flat and the decreasing trend of ΔP_{boiler} intensifies, so that the η_{th} gradually reaches its peak and then turns down. However, when $T_{5,op}$ and $P_{5,op}$ are used, ΔP_{boiler} can be effectively reduced, minimizing the negative impact on system performance. Consequently, the negative effect is consistently smaller than the positive effect when W_{net} is increased in the range of (100–1000) MWe. These optimization effects collectively contribute to a monotonically increasing η_{th} curve. Ref. [8]'s Fig. 2 elucidates the correlation between capacity and efficiency in water-steam cycles. As the unit capacity escalates, it affords larger flow channels and heat transfer surfaces, while mitigating the detrimental impact of boiler pressure drop penalties, thereby rendering larger capacity cycles inherently more efficient than their smaller counterparts. In this study, we optimize the main steam parameters specific to the sCO2 cycle's capacity, effectively mitigating the negative consequences of boiler pressure drop penalties and aligning the capacity-efficiency relationship of the sCO2 cycle more closely with that observed in water-steam cycles.

As depicted in Fig. 13b, $I/W_{\rm net}$ of all components exhibited a decreasing trend with increasing $W_{\rm net}$. The enhancement of efficiency of turbomachines lead to a reduction in $I_{\rm T}$ + $_{\rm C}/W_{\rm net}$, moreover, the suppressed boiler pressure drop causes a decreasing trend for $I_{\rm boiler}/W_{\rm net}$. Consequently, $I_{\rm total}/W_{\rm net}$, which is the sum of all the component terms, demonstrates a monotonic decrease. Within constant primary steam

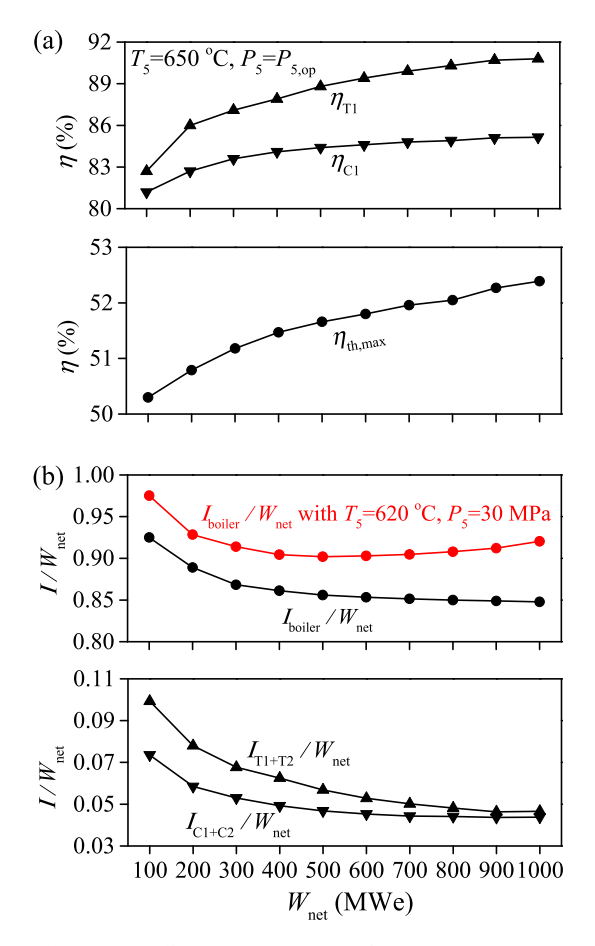


Fig. 13. (a) Efficiencies versus $W_{\rm net}$. (b) $I/W_{\rm net}$ versus $W_{\rm net}$.

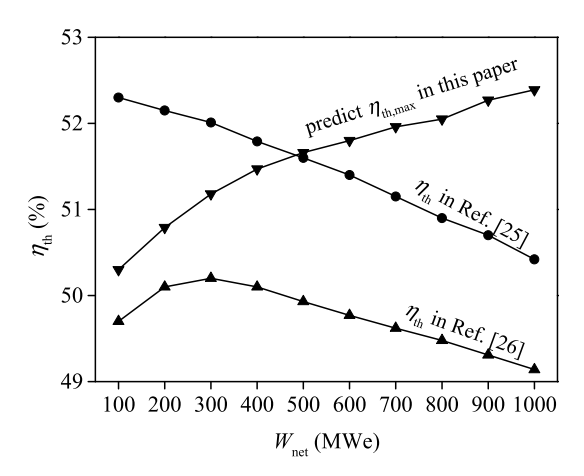


Fig. 14. $\eta_{\rm th}$ versus $W_{\rm net}$ relations under different researches.

conditions (P=30 MPa, $T=620\,^{\circ}$ C), the term $I_{\rm boiler}/W_{\rm net}$ is depicted by the red curve, with the discernible separation between curves underscoring that the pivotal factor driving the enhancement in $\eta_{\rm th}$ through optimized steam parameters is the substantial diminution of $I_{\rm boiler}/W_{\rm net}$. Consequently, the primary strategic focus of cycle optimization ought to be minimizing $I_{\rm boiler}$. Additionally, the significance of $I_{\rm T1+T2}$ and $I_{\rm C1+C2}$ becomes more pronounced in lower-capacity cycles, thereby rendering their optimization redundant within the 600–1000 MWe capacity range. These insights provide guidance in selecting optimization variables, facilitating targeted and refined enhancements in the performance of cycle systems.

In the concluding section, we briefly discuss the disparities in

findings across different studies (see Fig. 14) to inform future research directions. Liu [24] overlooked $\eta_{\rm T}$ and $\eta_{\rm C}$ variations with $W_{\rm net}$, leading to a $\Delta P_{\rm boiler}$ -dominated cycle performance and a negative correlation between $\eta_{\rm th}$ and $W_{\rm net}$. Wang [25] incorporated models of turbines and recuperaters, elucidating how the favourable influence of $\eta_{\rm T}$ and the detrimental effect of $\Delta P_{\rm boiler}$ on the cycle's performance fluctuate with varying capacities. Consequently, the $\eta_{\rm th}$ curve manifested a parabolic shape, achieving its apex at 300 MWe under the PFM flow strategy. Our research consolidates all models and implements optimized parameters ($T_{\rm 5,op}$) and $P_{\rm 5,op}$), which successfully counteracts the detrimental pressure drop penalty, ultimately outweighed by the collective beneficial impacts of enhanced $\eta_{\rm T}$ and $\eta_{\rm C}$ across the entire capacity spectrum. As a result, $\eta_{\rm th}$ exhibits a monotonic increase with $W_{\rm net}$.

The parabolic character of the thermal efficiency curve indicates that the adjustment strategy for the rated thermal parameters needs to be extremely careful when optimizing the performance of the unit. The complexity of the optimization scheme is higher when more factors are considered. Taking China's ultra-supercritical units as an example [61], when the rated pressure P_5 is increased from 25 MPa to 28 MPa, η_{th} is relatively increased by 0.45 %, but accompanied by a significant increase in the wall thickness of the boiler's pressure-bearing parts, the main steam pipes, and the valves, which leads to an average increase in the overall investment cost of about 4 %. In addition, ref. [61] reveals that under part-load conditions, η_{th} with $P_5 = 28$ MPa decreases instead. This highlights the complexity of the impact of P_5 , T_5 and W_{net} on system performance, and the actual optimization needs to comprehensively consider factors such as rated operating conditions, part-load conditions and total system cost. In this paper, a series of optimization results were obtained by focusing on the rated operating conditions (design point), but it should be noted that the optimization results may change when considering the part-load performance. Therefore, future research should aim at integrating the performance of units with various rated conditions under part-load, in order to obtain an optimization strategy that is closer to the engineering reality.

4. Conclusions

In this study, a comprehensive model encompassing a cycle system, π -type boiler, axial turbine, axial compressor, and recuperator was developed. The overlap energy utilization technique absorbs flue gas energies over entire temperature range, integrating various heater modules of the sCO₂ boiler to decrease large pressure drop induced efficiency penalty. The multi-stages axial turbines were modeled to explore their performance as $W_{\rm net}$ changes. Conclusions can be drawn as follows.

- 1. For a given capacity of 300 MWe, it is observed that η_{th} exhibits a parabolic trend with increasing P_5 , due to the tradeoff between the decreased pressure drop of sCO₂ boilers and the increased compression power. Additionally, η_{th} monotonically increases with T_5 , primarily attributed to the decrease in m, leading to a monotonous reduction in pressure drop of sCO₂ boilers.
- 2. Based on correlation analysis between $\eta_{\rm th}$ and P_5 , T_5 , we identified optimal main steam parameters $P_{5,\rm op}$ and $T_{5,\rm op}$ for ten capacity samples ranging from 100 to 1000 MWe. Notably, $P_{5,\rm op}$ increases monotonically from 26 to 37 MPa, due to the decreased pressure drops of sCO₂ boiler as positive effect suppressing the increased compression power as negative effect. Additionally, $T_{5,\rm op}$ is fixed at 650 °C, given by the tolerance limit of materials.
- 3. By optimizing the main steam parameters, it is demonstrated that η_{th} , $_{\text{max}}$ increases monotonically from 50.30 % to 52.39 % as W_{net} increases. This trend is primarily owing to the increased η_{T} and η_{C} as positive effect outweighing the increased pressure drops of sCO₂ boiler as negative effect.
- 4. After optimization of the main steam parameters, η_{th} is improved due to the effective reduction of pressure drops of sCO₂ boiler. Our work

concludes important roles of components' performance on system efficiencies, providing the guidance to select the "optimal" main steam parameters.

CRediT authorship contribution statement

Tianze Wang: Writing – original draft, Software, Methodology, Investigation. **Jinliang Xu:** Writing – review & editing, Methodology, Funding acquisition. **Guanglin Liu:** Writing – review & editing, Supervision, Conceptualization.

Declaration of competing interest

We state that the manuscript titled as "Maximum thermal efficiencies of supercritical CO2 power cycle at various power capacities" by Tianze Wang, Jinliang Xu, Guanglin Liu does not have any conflict of interest including any financial, personal or other relationships with other people or organizations within three years of beginning the submitted work that could inappropriately influence, or be perceived to influence, the present work.

Acknowledgements

This work was supported by the Natural Science Foundation of China (52130608, 51821004).

Data availability

Data will be made available on request.

References

- [1] Su CW, Pang LD, Qin M, Lobont OR, Umar M. The spillover effects among fossil fuel, renewables and carbon markets: evidence under the dual dilemma of climate change and energy crises. Energy 2023;274:127304.
- [2] Zhu L, Zheng W, Wang W, Zhong Z, Guo J, Song J. Study of load adjustment strategy for nuclear power units focusing on rankine cycle: flexibility-environment-economy. Energies 2024;17(6):1357.
- [3] Ma T, Li M, Xu J, Ni J, Tao W, Wang L. Study of dynamic response characteristics of S-CO2 cycle in coal-fired power plants based on real-time micro-grid load and a novel synergistic control method with variable working conditions. Energy Convers Manag 2022;254:115264.
- [4] Zhao Q, Xu J, Hou M, Chong D, Wang J, Chen W. Dynamic characteristic analysis of SCO2 Brayton cycle under different turbine back pressure modes. Energy 2024; 293:130563.
- [5] Li H, Fan G, Cao L, Yang Y, Yan X, Dai Y, et al. A comprehensive investigation on the design and off-design performance of supercritical carbon dioxide power system based on the small-scale lead-cooled fast reactor. J Clean Prod 2020;256: 120720.
- [6] Jin F, Chen D, Hu L, Huang Y, Bu S. Optimization of zigzag parameters in printed circuit heat exchanger for supercritical CO2 Brayton cycle based on multi-objective genetic algorithm. Energy Convers Manag 2022;270:116243.
- [7] Luo Q, Li X, Luo L, Du W, Yan H. Multi-objective performance analysis of different SCO2 Brayton cycles on hypersonic vehicles. Energy 2024:131624.
- [8] Bejan A, Lorente S, Yilbas BS, Sahin AZ. The effect of size on efficiency: power plants and vascular designs. Int J Heat Mass Tran 2011;54(7–8):1475–81.
- [9] Lam PL, Shiu A. A data envelopment analysis of the efficiency of China's thermal power generation. Util Policy 2001;10(2):75–83.
- [10] Ma Z, Deng J, Li Z, Li Q, Zhao P, Wang L, et al. Characteristics of NOx emission from Chinese coal-fired power plants equipped with new technologies. Atmos Environ 2016;131:164–70.
- [11] Franco A, Diaz AR. The future challenges for "clean coal technologies": joining efficiency increase and pollutant emission control. Energy 2009;34(3):348–54.
- [12] Xu Y, Yang CJ, Xuan X. Engineering and optimization approaches to enhance the thermal efficiency of coal electricity generation in China. Energy Pol 2013;60: 356–63.
- [13] Sun E, Wang X, Qian Q, Li H, Ma W, Zhang L, et al. Proposal and application of supercritical steam Rankine cycle using supercritical reheating regeneration process and its comparison between S-CO2 Brayton cycle. Energy Convers Manag 2023;280:116798.
- [14] Wang Y, Wang M, Wang D, Chang Y. Stochastic configuration network based cascade generalized predictive control of main steam temperature in power plants. Inf Sci 2022;587:123–41.
- [15] Cao Z, Yang S, Xiao H. Study of parameter and capacity of USC unit development in China. Pow Syst Eng 2007;2007(5):41–42+48 [in Chinese].

[16] Zhang S, Li Y, Liu X, Jiang Y. Gas-steam combined cycle system design and steam system parameter analysis study. Gas Turb Technol 2002;2002(3):44–8 [in Chinese].

- [17] Karthikeyan B, Kumar P, Narayanan R, Saravanan R, Coronas A. Thermo-economic optimization of hybrid solar-biomass driven organic rankine cycle integrated heat pump and PEM electrolyser for combined power, heating, and green hydrogen applications. Energy 2024:131436.
- [18] Xu J, Sun E, Li M, Liu H, Zhu B. Key issues and solution strategies for supercritical carbon dioxide coal fired power plant. Energy 2018;157:227–46.
- [19] Chen J, Cheng K, Li X, Huai X, Dong H. Thermodynamic evaluation and optimization of supercritical CO2 Brayton cycle considering recuperator types and designs. J Clean Prod 2023;414:137615.
- [20] Wang T, Xu J, Wang Z, Zheng H, Qi J, Liu G. Irreversible losses, characteristic sizes and efficiencies of sCO2 axial turbines dependent on power capacities. Energy 2023;275:127437.
- [21] Zhou T, Liu Z, Li X, Zhao M, Zhao Y. Thermodynamic design space data-mining and multi-objective optimization of SCO2 Brayton cycles. Energy Convers Manag 2021; 249:114844.
- [22] Yun S, Zhang D, Li X, Zhou X, Jiang D, Lv X, et al. Design, optimization and thermodynamic analysis of SCO2 Brayton cycle system for FHR. Prog Nucl Energy 2023;157:104593.
- [23] Alawadhi K, Alfalah A, Bader B, Alhouli Y, Murad A. An optimization study to evaluate the impact of the supercritical CO2 Brayton cycle's components on its overall performance. Appl Sci 2021;11(5):2389.
- [24] Liu C, Xu J, Li M, Wang Z, Xu Z, Xie J. Scale law of sCO2 coal fired power plants regarding system performance dependent on power capacities. Energy Convers Manag 2020;226:113505.
- [25] Wang Z, Xu J, Wang T, Miao Z, Wang Q, Liu G. Performance of sCO2 coal-fired power plants at various power capacities. J Clean Prod 2023;416:137949.
- [26] Jin Q, Xia S, Chen L. A modified recompression S-CO2 Brayton cycle and its thermodynamic optimization. Energy 2023;263:126015.
- [27] Yang J, Yang Z, Duan Y. Part-load performance analysis and comparison of supercritical CO2 Brayton cycles. Energy Convers Manag 2020;214:112832.
- [28] Khan Y, Mishra RS. Performance analysis of solar driven combined recompression main compressor intercooling supercritical CO2 cycle and organic Rankine cycle using low GWP fluids. Energy Built Environ 2022;3(4):496–507.
- [29] Sun E, Xu J, Li M, Liu G, Zhu B. Connected-top-bottom-cycle to cascade utilize flue gas heat for supercritical carbon dioxide coal fired power plant. Energy Convers Manag 2018;172:138–54.
- [30] Xu J, Liu C, Sun E, Xie J, Li M, Yang Y, et al. Perspective of S—CO2 power cycles. Energy 2019:186:115831.
- [31] Zhu M, Zhou J, Su S, Xu J, Li A, Chen L, et al. Study on supercritical CO2 coal-fired boiler based on improved genetic algorithm. Energy Convers Manag 2020;221: 113163.
- [32] Wang Z, Zheng H, Xu J, Li M, Sun E, Guo Y, et al. The roadmap towards the efficiency limit for supercritical carbon dioxide coal fired power plant. Energy Convers Manag 2022;269:116166.
- [33] Sultan JN, Abbas MK, Abd-al KIM, Karash ET, Ali AM, Ibrhim HA. Corrosion behavior of thermal seamless carbon steel boiler pipes. Ann Chimie Sci Matériaux 2021;21.
- [34] Moisseytsev A, Sienicki JJ. Development of a plant dynamics computer code for analysis of a supercritical carbon dioxide Brayton cycle energy converter coupled to a natural circulation lead-cooled fast reactor (No. ANL-06/27). Argonne, IL: Argonne National Lab; 2007.
- [35] Aungier RH. Turbine Aerodynamics: Axial-flow and radial-inflow turbine design and analysis. New York (USA): ASME Press; 2005.
- [36] Bidkar RA, Mann A, Singh R, Sevincer E, Cich S, Day M, et al. Conceptual designs of 50 MWe and 450 MWe supercritical CO2 turbomachinery trains for power generation from coal. Part 1: cycle and turbine. 5th International symposiumsupercritical CO2 2016;2:28–31.
- [37] Da Lio L, Manente G, Lazzaretto A. Predicting the optimum design of single stage axial expanders in ORC systems: is there a single efficiency map for different working fluids? Appl Energy 2016;167:44–58.
- [38] Da Lio L, Manente G, Lazzaretto A. New efficiency charts for the optimum design of axial flow turbines for organic Rankine cycles. Energy 2014;77:447–59.
- [39] Salah SI, White MT, Sayma AI. A comparison of axial turbine loss models for air sCO2 and ORC turbines across a range of scales. Int J Thermofluids 2022;15: 100156.
- [40] Peng N, Wang E, Wang W. Design and analysis of a 1.5 kW single-stage partialadmission impulse turbine for low-grade energy utilization. Energy 2023;268: 126631.
- [41] Salah SI, Crespi F, White MT, Muñoz A, Paggini A, Ruggiero M, et al. Axial turbine flow path design for concentrated solar power plants operating with CO2 blends. Appl Therm Eng 2023;230:120612.
- [42] Liu Z, Luo W, Zhao Q, Zhao W, Xu J. Preliminary design and model assessment of a supercritical CO2 compressor. Appl Sci 2018;8(4):595.
- [43] Park JH, Park HS, Kwon JG, Kim TH, Kim MH. Optimization and thermodynamic analysis of supercritical CO2 Brayton recompression cycle for various small modular reactors. Energy 2018;160:520–35.
- [44] Salah S. Design and analysis of supercritical carbon-dixoide axial turbines. City: University of London; 2023.
- [45] Kadivar M, Tormey D, McGranaghan G. A review on turbulent flow over rough surfaces: fundamentals and theories. Int J Thermofluids 2021;10:100077.
- [46] Linares JI, Montes MJ, Cantizano A, Sánchez C. A novel supercritical CO2 recompression Brayton power cycle for power tower concentrating solar plants. Appl Energy 2020;263:114644.

- [47] Aungier RH, Farokhi S. Axial-flow compressors: a strategy for aerodynamic design and analysis. Appl Mech Rev 2004;57(4):B22–3.
- [48] Wang Y, Guenette G, Hejzlar P, Driscoll M. Compressor design for the supercritical CO2 Brayton cycle. In: 2nd international energy conversion engineering conference. Providence, Rhode Island; August, 2004. p. 16–9.
- [49] Allison T, Wilkes J, Brun K, Moore J. Turbomachinery overview for supercritical CO2 power cycles. Proceedings of the 46th turbomachinery symposium. Turbomachinery laboratory, Texas A&M engineering experiment station. 2017.
- [50] Boyce MP. Axial-flow compressors. Gas Turbine Engineering Handbook 2012: 303–55.
- [51] Jing Q, Xie Y, Zhang D. Thermal hydraulic performance of printed circuit heat exchanger with various channel configurations and arc ribs for SCO2 Brayton cycle. Int J Heat Mass Tran 2020;150:119272.
- [52] Niu X, Liu J, Yue G, Li H, Qi L, Hong W. Numerical study on the flow and heat transfer performance of SCO2/molten salt in Z-type printed circuit heat exchangers. Appl Therm Eng 2024;247:123015.
- [53] Huang C, Cai W, Wang Y, Liu Y, Li Q, Li B. Review on the characteristics of flow and heat transfer in printed circuit heat exchangers. Appl Therm Eng 2019;153: 190–205.

- [54] Siddiqui ME, Almitani KH. Energy analysis of the S-CO2 Brayton cycle with improved heat regeneration. Processes 2018;7(1):3.
- [55] Yin JM, Bullard CW, Hrnjak PS. Pressure drop measurements in microchannel heat exchanger. Air conditioning and refrigeration center CR-30. 2000.
- [56] Shi D, Zhang L, Xie Y, Zhang D. Aerodynamic design and off-design performance analysis of a multi-stage S-CO2 axial turbine based on solar power generation system. Appl Sci 2019;9(4):714.
- [57] Wang J, Sun Z, Dai Y, Ma S. Parametric optimization design for supercritical CO2 power cycle using genetic algorithm and artificial neural network. Appl Energy 2010;87(4):1317–24.
- [58] Shen Q, Cheng J. Optimizing analysis of the parameters and thermal system for ultra supercritical unit. Power Eng 2004;(3):305–310+405 [in Chinese].
- [59] Liu M, Zhang X, Yang K, Wang B, Yan J. Comparison and sensitivity analysis of the efficiency enhancements of coal-fired power plants integrated with supercritical CO2 Brayton cycle and steam Rankine cycle. Energy Convers Manag 2019;198: 111918
- [60] Sarkar J, Bhattacharyya S. Optimization of recompression S-CO2 power cycle with reheating. Energy Convers Manag 2009;50(8):1939–45.
- [61] Cao Z, Tang S, Xiao H. Study of parameter and capacity of USC unit development in China. Pow Syst Eng 2007;(5):41–42+48 [in Chinese].